A Novel Scheme of Multicarrier Modulation with the Discrete Cosine Transform

María Elena Domínguez-Jiménez, David Luengo, Gabriela Sansigre-Vidal, Fernando Cruz-Roldán, *Senior Member, IEEE.*

***Abstract*—In this work, we derive a novel multicarrier modulation based on the Type-I even discrete cosine transform (DCT1e), which includes new procedures to carry out both the channel estimation and the signal reconstruction. By using a small number of training symbols, we achieve an accurate estimation of the channel's impulse response (CIR) using a novel mirror, replicate and add (MIRA) procedure. The proposed scheme does not require knowing the length of the CIR and is valid even in the presence of spectral nulls. We provide the theoretical results that guarantee the validity of the developed technique. After the estimation process, the transmitted symbols are also reconstructed by means of the DCT1e using the same novel MIRA scheme. The conditions that ensure a perfect reconstruction in the absence of noise are also provided in this case. Numerical simulations illustrate the excellent behaviour of the proposed approach, both in terms of channel estimation and recovery of the transmitted information.**

***Index Terms*—Multicarrier modulation; discrete cosine transform (DCT); channel estimation; signal reconstruction**

I. INTRODUCTION

Multicarrier modulation (MCM) is the preferred medium-access technique in many current state-of-the-art digital communication systems [1]. Instead of the discrete Fourier transform (DFT), which has been adopted in most of the standards, several authors have studied the benefits of using the discrete cosine transform (DCT) as the basis of alternative MCM schemes [2]–[10]. DCT-based systems exhibit excellent spectral compaction and energy concentration, which lead to less interference leakage to adjacent subcarriers [3], [11], as well as better performance under carrier frequency offset (CFO) [2], [4], [6], [12]. They also offer comparable complexity to DFT-based systems for long channels and reduced power consumption for real constellations [2].

Channel estimation is essential in digital communication systems, especially in DCT-based transceivers that employ a front-end pre-filter at the receiver [2], [4], [6], [13]. The channel's impulse response (CIR) is usually time-varying, and thus it is necessary to re-estimate the CIR from time to time. To this aim, some training or pilot symbols, which are known by both the transmitter and the receiver, are frequently used. In MCM systems, channel estimation has typically required the use of the DFT, both in the case of orthogonal frequency division multiplexing (OFDM) schemes (see, e.g., [14], [15] and references therein) and in DCT-based systems [16]–[19].

However, several works have recently addressed the channel estimation problem using the DCT instead of the DFT. First of all, a compressed channel sensing (CCS) method using the DCT1e was already proposed in [20]. Unfortunately, this technique is only valid for channels with symmetric CIR, which is not the case in most practical applications. In order to overcome this limitation, [12] developed a novel channel estimator for the Type-II even and the Type-IV even DCTs (DCT2e and DCT4e respectively). The key idea of [12] was constructing a symmetric training signal, thus freeing the channel's CIR from the symmetry restriction. This estimator has then been extended to the DCT1e in [21], as well as the DCT3e [13], [22]–[24]. The transmission scheme of the above systems still requires the use of redundant samples, such as symmetric extension or zero padding, inserted at each transmitted data symbol.

This work presents a novel scheme based on the DCT1e, both for channel estimation and signal reconstruction, that outperforms the ones proposed in [21], [25]. The major contributions of this work are:

1) We derive the conditions to perform the transmission channel partition with zeros, without using symmetric extension into each time-domain data symbol. In addition, we show how to correct the channel effects with only one-coefficient per subchannel equalizer.
2) We develop a novel mirror, replicate and add (MIRA) procedure for channel estimation, with two important advantages over the method proposed in [21]. On the one hand, this new scheme can be applied without prior knowledge of the maximum length of the channel's impulse response. On the other hand, the training symbols can be chosen in a more general way: they do not need to contain many zero coefficients in the transformed domain. Finally, the simulations (see Section VI) also show that the novel approach outperforms the one in [21] in terms of normalised mean squared error (NMSE).
3) We provide theoretical results that guarantee the validity of the proposed technique.
4) We also consider the signal reconstruction problem (i.e., the estimation of the transmitted symbols) by means of the DCT1e. Unlike the approach given in [25], where a symmetric extension was imposed, here we provide a solution that only introduces some null components. By exploiting the same MIRA procedure, we demon-

M.E. Domínguez-Jiménez, D. Luengo and G. Sansigre-Vidal are members of the TACA Research Group of Universidad Politécnica de Madrid (Spain) (emails: {elena.dominguez,david.luengo,gabriela.sansigre}@upm.es).

F. Cruz-Roldán is with Universidad de Alcalá (Spain) (email: fernando.cruz@uah.es).

This work has been partly funded by the Spanish Ministry of Economy and Competitiveness through projects TEC2015-64835-C3-1-R and TEC2015-64835-C3-3-R.

strate that our novel scheme guarantees perfect signal reconstruction in the absence of noise.

We focus on the DCT1e due to the following important properties:

- The direct and the inverse DCT1e are defined by the same expression except for a scaling factor that can be normalized [26]. This characteristic simplifies the implementation of the system, since exactly the same hardware can be used to carry out the transform blocks at both the transmitter and the receiver.
- The convolution of two vectors is transformed by the DCT1e into a pointwise product of their transforms under some symmetry conditions on one of the vectors [26], [27]. This property is shared by other DCTs (although the symmetry conditions may differ) and is analogous to the circular convolution property of the DFT. This is the key property for channel estimation and signal reconstruction in MCM systems, since it enables the estimation of non-symmetric channels without introducing any additional transform in the receiver by constructing a symmetric training signal [12].
- Signals which present whole-point symmetry (WS), a.k.a antisymmetry, are transformed into vectors with a high number of zero coefficients in the DCT1e transform domain (and viceversa). This advantage ensures that the signals obtained are sparse and can be exploited to develop compressed channel sensing schemes, as already done in [20] for symmetric channels.
- Regarding computational issues, in [28], [29] it is claimed that the DCT1e of length N is equivalent to a DFT of length $2N$ with real-symmetric input data. Furthermore, the authors establish that the multiplication complexity of the DCT1e algorithm can be saved, starting from their new FFT with an identical approach.

The rest of the paper is organized as follows. First of all, in Section II an overview of the novel system is provided: the block diagram of the proposed transceiver is introduced and a general description of the different blocks is given. Then, some key properties of the DCT1e are reviewed in Section III. This is followed by the two main sections from a theoretical point of view. On the one hand, the channel estimation problem is addressed in Section IV: the newly proposed channel estimation procedure (MIRA) is described in Section IV-A, and the theoretical justification is provided in Section IV-B. On the other hand, Section V explains how to recover any transmitted information symbol by means of the DCT1e using the novel MIRA procedure introduced in Section IV-A and provides the theoretical conditions for a perfect reconstruction in the absence of noise. Finally, Section VI contains several numerical examples that illustrate the excellent behaviour of the proposed communications system for several channels and subcarrier modulation schemes, and the main contributions of this work are highlighted in Section VII.

The notation used in this paper is as follows. Bold-face letters indicate vectors (lower case) and matrices (upper case). The transpose of $\mathbf{A}$ is denoted by $\mathbf{A}^T$ and $\mathbf{I}_N$ represents the $N \times N$ identity matrix. The subscript is omitted whenever the size is clear from the context. $\mathbf{J}$ stands for the counter-identity matrix, and $\mathbf{0}_{M\times N}$ denotes an $M \times N$ matrix of zeros.

II. System Overview

The block diagram of the proposed DCT-based MCM transceiver is shown in Figure 1. Note that the receiver includes two separate parts: one for channel estimation and another one for signal reconstruction. We consider a synchronous communications system, where symbols are organised in frames of F symbols, as shown in Figure 2, with an initial training symbol ($S_{i,0}$ with i denoting the frame number) devoted to CIR estimation and the remaining $F-1$ symbols ($S_{i,1}, \ldots, S_{i,F-1}$) to data transmission.

In the transmitter, the N-length pilot/training symbol in each frame, $\mathbf{x}^{(\text{ps})}$, is stored in memory and directly injected in the second block, as shown in Figure 1. For the remaining data symbols in the frame, an inverse transform ($\mathbf{T}_a^{-1}$) is applied to the original data vector, $\mathbf{X} = [X_0, X_1, \ldots, X_{N-1}]^T$, in order to obtain the time-domain data vector: $\mathbf{x} = [x_0, x_1, \ldots, x_{N-1}]^T$. Here, we use the inverse DCT1e, implying that $\mathbf{T}_a^{-1} = \mathbf{C}_{1e}^{-1} = \mathbf{C}_{1e}$, with $\mathbf{C}_{1e}$ denoting the DCT1e transform matrix, which is defined by (1) and (2) and whose properties are detailed in Section III. Then, in order to avoid intersymbol interference during synchronous transmission, matrix $\mathbf{\Gamma}$ introduces guard intervals composed of $L-1$ zeros, with L denoting the maximum length of the channel's impulse response, at each side of the signal $\mathbf{x}$:

$$\mathbf{x}_e = \mathbf{\Gamma} \cdot \mathbf{x} = \begin{bmatrix} \mathbf{0}_{(L-1)\times N} \\ \mathbf{I}_N \\ \mathbf{0}_{(L-1)\times N} \end{bmatrix} \cdot \mathbf{x}.$$

The samples of this extended vector, $\mathbf{x}_e$, are transmitted through the $L-$length CIR given by $\mathbf{h}_{\text{ch}} = [h_0, \ldots, h_{L-1}]^T$, with $L < N-2$. The central part of the received signal (which contains the samples required for channel estimation and signal reconstruction) is thus $\mathbf{y} = \mathbf{x} * \mathbf{h}_{\text{ch}} + \mathbf{z}$, of length $L+N-1$, where $\mathbf{z}$ is the additive white Gaussian noise (AWGN) vector and $*$ denotes the standard linear convolution operator.

In the receiver, the first goal is to estimate the CIR, $\mathbf{h}_{\text{ch}}$. In order to achieve this aim, a known pilot/training sequence $\mathbf{x}^{(\text{ps})}$ is transmitted in the first symbol of each frame, as previously indicated, and the received signal is processed using the block diagram in the upper part of the receiver (see Figure 1). First of all, the MIRA scheme, which amounts to a linear transformation using the matrix $\mathbf{\Upsilon}$ defined in (12), is applied to $\mathbf{y}$ (of length $L+N-1$), thus obtaining a shortened vector $\mathbf{y}_{\text{m}}$ of length N (see Section IV for further details). Then, an appropriate direct transform ($\mathbf{T}_c$) is applied to $\mathbf{y}_{\text{m}}$ in order to obtain the transformed received symbols $\mathbf{Y}_{\text{m}} = [Y_{m,0}, Y_{m,1}, \ldots, Y_{m,N_0-1}]$. In this case, $\mathbf{T}_c = \mathbf{T}_a^{-1} = \mathbf{C}_{1e}$ due to the properties of the DCT1e discussed in Section III, so the same transform used in the transmitter can be applied for channel estimation in the receiver. Next, the single frequency equalization coefficients, $\mathbf{d}^{(\text{ps})} = [d_0^{(\text{ps})}, d_1^{(\text{ps})}, \ldots, d_{N_0-1}^{(\text{ps})}]^T$ are computed, using the simple procedure detailed in Section IV,

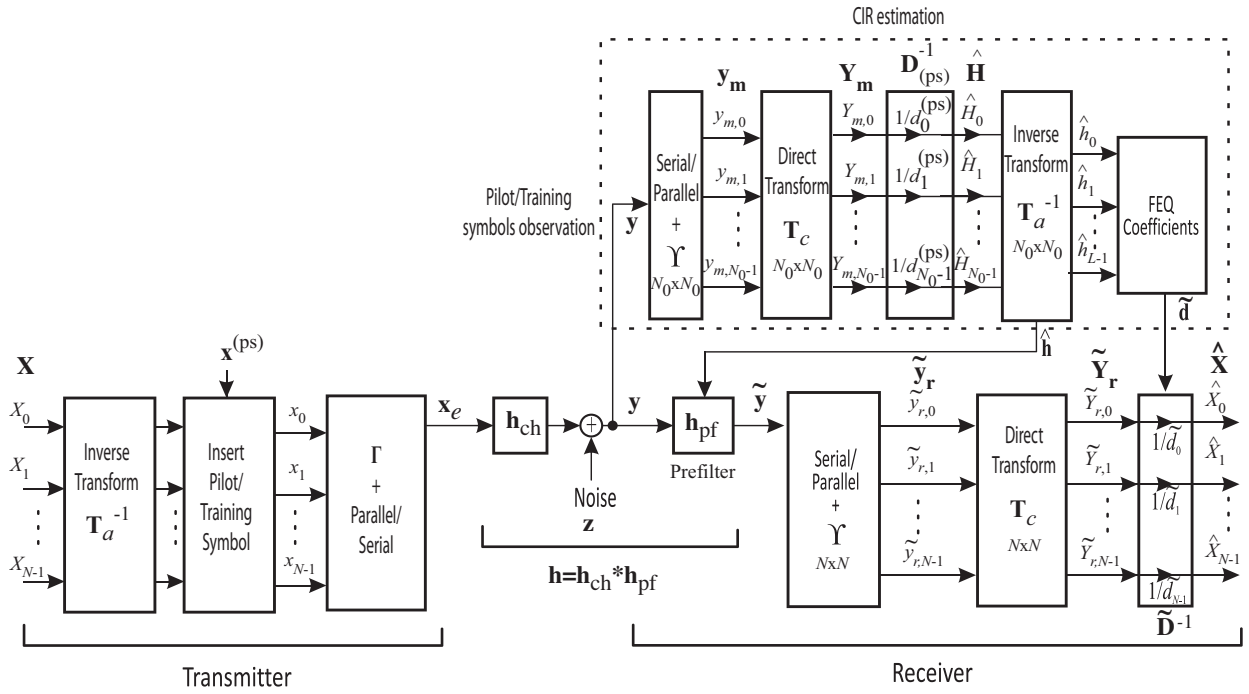

Fig. 1. General block diagram of the DCT1e-based MCM transceiver for channel estimation and signal reconstruction.

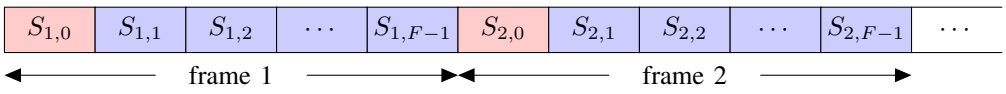

Fig. 2. Frame structure for the proposed DCT1e-based MCM scheme. Red boxes indicate the initial training symbol in each frame ($S_{i,0}$ with i denoting the frame number). Blue boxes indicate the remaining $F-1$ data symbols ($S_{i,1},\ldots,S_{i,F-1}$).

and used to perform the frequency equalization of the information symbols transmitted after the training stage. Finally, the estimated CIR, $\hat{\mathbf{h}}_{\text{ch}} = [\hat{h}_0,\ldots,\hat{h}_{L-1}]^T$, is obtained by applying the inverse transform $\mathbf{T}_a^{-1}$ to the estimated channel in the transformed domain $[\hat{H}_0,\ldots,\hat{H}_{N-1}]$. This estimated CIR is used both to construct the pre-filter $\mathbf{h}_{\text{pf}}$, required to guarantee a symmetric global CIR, $\mathbf{h} = \mathbf{h}_{\text{ch}} * \mathbf{h}_{\text{pf}}$, and to obtain the frequency equalization (FEQ) coefficients for the signal reconstruction stage, $\widetilde{\mathbf{d}} = [\widetilde{d}_0,\widetilde{d}_1,\ldots,\widetilde{d}_{N-1}]^T$. The whole process is detailed in Section IV.

After the channel has been estimated, the system is ready to start receiving data symbols. The central part of the received signal (which contains the samples required for signal reconstruction), $\widetilde{\mathbf{y}} = \mathbf{x}*\mathbf{h}+\mathbf{z}$ of length $2L+N-2$, is now processed using the block diagram in the lower part of the receiver. As in the channel estimation stage, we first apply MIRA in order to obtain an N-length signal $\widetilde{\mathbf{y}}_{\text{r}}$. This signal is then transformed using $\mathbf{T}_c = \mathbf{T}_a^{-1} = \mathbf{C}_{1e}$ and equalized using the coefficients $\widetilde{d}_k$ computed during the training stage, as shown in Figure 1. The whole signal reconstruction process is described in detail in Section V. Note that we use different values of N for the channel estimation ($N = N_0$ odd, as the transmitted signal has to have WS) and signal reconstruction ($N = N_0+1$ even, as in most MCM schemes) stages. Let us remark again that the channel estimation (which requires an odd value of N) is performed only once per frame, whereas the reconstruction stage (where $N = 2^n$ and fast DCT1e algorithms can be used) is carried out most of the time.

III. The Discrete Cosine Transform Type-I even

In this Section we recall the definition of the DCT1e matrix, and give some properties that will be useful for the proposed MCM scheme. The DCT1e of an N-length signal is given by the matrix $\mathbf{C}_{1e}$:

$$[\mathbf{C}_{1e}]_{k,j} = a_j \cos\left(\frac{kj\pi}{N-1}\right),\ 0 \le k,j \le N-1, \quad (1)$$

where

$$a_j = \begin{cases} \frac{1}{\sqrt{2(N-1)}}, & \text{if} \quad j = 0, N-1; \\ \frac{2}{\sqrt{2(N-1)}}, & \text{otherwise.} \end{cases} \quad (2)$$

This is the definition of $\mathbf{C}_{1e}$ given in [26], except for the normalization factor $\sqrt{2(N-1)}$, which has been introduced here in order to ensure the involution property: $\mathbf{C}_{1e}^{-1} = \mathbf{C}_{1e}$, which simplifies the numerical calculations. This way, the inverse and direct DCT1e transforms are equal.

Notice that DCT1e also presents the following properties:

1) *Property 1:* The DCT1e of a vector $\mathbf{x} = [x_0,\cdots,x_{N-1}]^T$ is related to the DCT1e of its reversed version $\mathbf{J}\cdot\mathbf{x} = [x_{N-1},\cdots,x_0]^T$ as follows: $\mathbf{C}_{1e}\cdot\mathbf{x}$ and $\mathbf{C}_{1e}\cdot\mathbf{J}\cdot\mathbf{x}$ have the same even-indexed components, whereas their odd-indexed components

have opposite signs. In other words, their $m-$th components are related by:

$$[\mathbf{C}_{1e}\cdot\mathbf{J}\cdot\mathbf{x}]_m=(-1)^m\,[\mathbf{C}_{1e}\cdot\mathbf{x}]_m\,,\ m=0,\ldots,N-1.$$

The reason is that

$$\begin{aligned}&[\mathbf{C}_{1e}\cdot\mathbf{J}]_{m,n}=[\mathbf{C}_{1e}]_{m,N-1-n}\\&=a_{N-1-n}\cos\left(\frac{m(N-1-n)\pi}{N-1}\right)\\&=a_n\cos\left(m\pi-\frac{mn\pi}{N-1}\right)\\&=a_n\,(-1)^m\cos\left(\frac{mn\pi}{N-1}\right)=(-1)^m\,[\mathbf{C}_{1e}]_{m,n}\,.\end{aligned}$$

Therefore, if $\mathbf{C}_{1e}\cdot\mathbf{x}=[X_0,X_1,X_2,\cdots,X_{N-1}]$, then

$$\mathbf{C}_{1e}\cdot(\mathbf{x}+\mathbf{J}\cdot\mathbf{x})=2[X_0,0,X_2,0,\cdots],\tag{3}$$

$$\mathbf{C}_{1e}\cdot(\mathbf{x}-\mathbf{J}\cdot\mathbf{x})=2[0,X_1,0,X_3,\cdots].\tag{4}$$

2) *Property 2:* DCT1e transforms symmetric signals into vectors with null odd-indexed components. In fact, if $\mathbf{V}$ is a vector with zero odd-indexed components,

$$\mathbf{V}=[V_0,0,V_2,0,\cdots],$$

then Equation (3) guarantees that $\mathbf{C}_{1e}^{-1}\cdot\mathbf{V}=\mathbf{v}$ is a symmetric vector (say, $\mathbf{J}\cdot\mathbf{v}=\mathbf{v}$). In case N is even ($N=2M$, where M is an integer), then $\mathbf{v}$ presents half-point symmetry (HS), of the kind $\mathbf{v}=[v_0,\cdots,v_{M-1},v_{M-1},\cdots,v_0]^T$. If N is odd ($N=2M+1$), then the symmetry of $\mathbf{v}$ is a whole-point symmetry (WS), of the kind

$$\mathbf{v}=[v_0,\cdots,v_{M-1},v_M,v_{M-1},\cdots,v_0]^T.$$

In the same way, from Equation (4) we derive that DCT1e transforms antisymmetric signals into vectors with null even-indexed components; for even length, the signals are half-point antisymmetric (HA) and for odd length, whole-point antisymmetric (WA).

3) *Property 3 (DCT1e and diagonalization):* In [27] it is shown that an $N\times N$ matrix $\mathbf{A}$ is diagonalized via $\mathbf{C}_{1e}$ if it can be split as $\mathbf{A}=\mathbf{G}+\mathbf{M}_{1e}$, where $\mathbf{G}$ is an $N\times N$ symmetric Toeplitz matrix given by

$$\mathbf{G}=\begin{bmatrix}t_0&t_1&\cdots&t_{N-2}&t_{N-1}\\t_1&\ddots&\ddots&&t_{N-2}\\\vdots&\ddots&\ddots&\ddots&\vdots\\t_{N-2}&&\ddots&\ddots&t_1\\t_{N-1}&t_{N-2}&\cdots&t_1&t_0\end{bmatrix},\tag{5}$$

and $\mathbf{M}_{1e}$ comes from a Hankel matrix whose first and last columns have been set to zero:

$$\mathbf{M}_{1e}=\begin{bmatrix}0&t_1&\cdots&t_{N-2}&0\\0&&\iddots&t_{N-1}&0\\0&t_{N-2}&\iddots&t_{N-2}&0\\0&t_{N-1}&\iddots&&0\\0&t_{N-2}&\cdots&t_1&0\end{bmatrix}.\tag{6}$$

Moreover, the eigenvalues of $\mathbf{A}$ are the N components of the vector $\mathbf{C}_{1e}\cdot[t_0,\cdots,t_{N-1}]^T$ [27, p. 2634].

4) *Property 4:* Any $L\times L$ submatrix of $\mathbf{C}_{1e}$, whose columns have been extracted from the first L columns of $\mathbf{C}_{1e}$, is invertible. [20, p. 3].

IV. DCT1e for Channel Estimation

A. Channel Estimation by MIRA-DCT1e procedure

We now focus on the channel estimation problem of Figure 1, by using the DCT1e at both the transmitter and the receiver: $\mathbf{T}_a^{-1}=\mathbf{T}_c=\mathbf{C}_{1e}$. Let $\mathbf{h}_{\text{ch}}=[h_0,\ldots,h_{L-1}]^T$, and let

$$\mathbf{x}^{(\text{ps})}=[0,x_{M-1},\cdots,x_1,x_0,x_1,\cdots,x_{M-1},0]^T\tag{7}$$

be the N-length pilot/training symbol to be transmitted[1]. Hereinafter, let us consider without loss of generality that $N=N_0=2M+1$, and $\left[\mathbf{x}^{(\text{ps})}\right]_0=\left[\mathbf{x}^{(\text{ps})}\right]_{2M}=0$. In this case, the $(N_0+2M)-$length received data vector can be obtained as $\mathbf{y}=\mathbf{x}^{(\text{ps})}*[\mathbf{h}_{\text{ch}}^T,0,\ldots,0]^T+\mathbf{z}$, which can be rewritten as

$$\mathbf{y}=\begin{bmatrix}0&0&\cdots&0\\x_{M-1}&0&\cdots&0\\\vdots&x_{M-1}&\ddots&\vdots\\x_1&\ddots&\ddots&0\\x_0&x_1&\ddots&x_{M-1}\\x_1&x_0&\ddots&\vdots\\\vdots&x_1&\ddots&x_1\\x_{M-1}&\ddots&\ddots&x_0\\0&x_{M-1}&\ddots&x_1\\\vdots&0&\ddots&\vdots\\0&\ddots&0&x_{M-1}\\0&0&\cdots&0\end{bmatrix}\begin{bmatrix}h_0\\\vdots\\h_{L-1}\\0\\\vdots\\0\end{bmatrix}+\mathbf{z}.\tag{8}$$

Equation (8) can be rewritten as

$$\mathbf{y}=\widetilde{\mathbf{X}}\cdot\mathbf{h}_{\text{zp}}+\mathbf{z},\tag{9}$$

in which we have

$$\mathbf{h}_{\text{zp}}=[0,\mathbf{h}_{\text{ch}}^T,0,\ldots,0]^T,\tag{10}$$

and $\widetilde{\mathbf{X}}$ is the Toeplitz matrix in (8) augmented with a first column on the left equal to

$$[x_{M-1},\cdots,x_1,x_0,x_1,\cdots,x_{M-1},0,\cdots,0]^T,$$

i.e., $\widetilde{\mathbf{X}}$ is an $(N+2M)\times N$ Toeplitz matrix with first row $[x_{M-1},0,\cdots,0]$ and first column $[x_{M-1},\cdots,x_1,x_0,x_1,\cdots,x_{M-1},0,\cdots,0]^T$.

The first (N_0+2M) components of the received data vector can be denoted as

$$\mathbf{y}=[y_{-M},\ldots,y_0,\ldots,y_{N_0-1},\ldots,y_{N_0+M-1}]^T.$$

[1]Observe that the symmetry of the pilot symbol can be employed for timing- and frequency- synchronization [30].

Now we need to define the auxiliary matrix $\boldsymbol{\Upsilon}$, which transforms such arbitrary vector $\mathbf{y}$ of length N_0+2M, into the following N_0-length vector:

$$\begin{aligned}\mathbf{y}_{\rm m} = \boldsymbol{\Upsilon}\cdot\mathbf{y} &= [y_0,...,y_{M-1},y_M,...,y_{N_0-M},...,y_{N_0-1}]^T + \\ &+[y_0,...,y_{1-M},0,...,0,y_{N_0+M-2},..,y_{N_0-1}]^T.\end{aligned} \tag{11}$$

Note that this modification, depicted in the block diagram of Figure 3, is performed as follows: after discarding the first and the last component of $\mathbf{y}$, i.e., y_{-M} and y_{N_0+M-1}, the following first M components are symmetrized as in a mirror, and added to their adjacent M components, where we have replicated y_0; in an analogous way, the last M components are symmetrized as in a mirror, and added to their previous M components, where we have replicated y_{N_0-1}. In other words, it is a *mirror, replicate and add* procedure, so we denote it as MIRA.

The explicit expression of the $N_0\times(N_0+2M)$ MIRA matrix is

$$\begin{aligned}\boldsymbol{\Upsilon} = &\left[\begin{array}{ccc}\mathbf{0}_{N_0\times M} & \mathbf{I}_{N_0} & \mathbf{0}_{N_0\times M}\end{array}\right] + \\ &+\left[\begin{array}{ccccc}\mathbf{0}_{M\times 1} & \mathbf{J}_M & \mathbf{0}_{M\times(N_0-2)} & \mathbf{0}_M & \mathbf{0}_{M\times 1}\\ \mathbf{0}_{N_0\times 1} & \mathbf{0}_{N_0\times M} & \mathbf{0}_{N_0\times(N_0-2)} & \mathbf{0}_{N_0\times M} & \mathbf{0}_{N_0\times 1}\\ \mathbf{0}_{M\times 1} & \mathbf{0}_M & \mathbf{0}_{M\times(N_0-2)} & \mathbf{J}_M & \mathbf{0}_{M\times 1}\end{array}\right].\end{aligned} \tag{12}$$

The aim of $\boldsymbol{\Upsilon}$ is to modify $\widetilde{\mathbf{X}}$ in order to obtain a matrix, namely $\mathbf{X}_{equiv}$, such that $\mathbf{T}\cdot\mathbf{X}_{equiv}\cdot\mathbf{T}^{-1}=\mathbf{D}_{\rm (ps)}$ is diagonal, containing the eigenvalues of $\mathbf{X}_{equiv}$. This matrix $\mathbf{X}_{equiv}$ shares with $\boldsymbol{\Upsilon}\cdot\widetilde{\mathbf{X}}$ all the columns unless first and last, as it is shown in the next result.

Proposition 1: Let us consider the $(N_0+2M)\times N_0$ convolution matrix $\widetilde{\mathbf{X}}$ and the $N_0\times(N_0+2M)$ MIRA matrix $\boldsymbol{\Upsilon}$ (12). There exists an $N_0\times N_0$ matrix $\mathbf{X}_{equiv}$ which is diagonalized by DCT1e, and that verifies, for any vector $\mathbf{b}$ of length N_0-2,

$$\mathbf{X}_{equiv}\cdot[0,\mathbf{b},0]^T=\boldsymbol{\Upsilon}\cdot\widetilde{\mathbf{X}}\cdot[0,\mathbf{b},0]^T.$$

Proof: It suffices to apply the MIRA procedure to the rows of $\widetilde{\mathbf{X}}$: by discarding the first and last row, we replicate two rows in matrix $\widetilde{\mathbf{X}}$ (namely the $(M+1)$-th and the N_0-th row), and then we reverse its first/last rows and add them to their adjacent ones. The obtained matrix can be easily written as $\boldsymbol{\Upsilon}\cdot\widetilde{\mathbf{X}}=\mathbf{X}_T+\mathbf{X}'_H$ being $\mathbf{X}_T$ and $\mathbf{X}'_H$, respectively, Toeplitz and Hankel matrices of the kind:

$$\mathbf{X}_T=\left[\begin{array}{ccccccc}x_0 & x_1 & \cdots & x_{M-1} & 0 & \cdots & 0\\ x_1 & \ddots & \ddots & & & \ddots & \vdots\\ \vdots & \ddots & \ddots & \ddots & & & 0\\ x_{M-1} & & \ddots & \ddots & & & x_{M-1}\\ 0 & & & & & & \vdots\\ \vdots & \ddots & & & & & x_1\\ 0 & \cdots & 0 & x_{M-1} & \cdots & x_1 & x_0\end{array}\right],$$

$$\mathbf{X}'_H=\left[\begin{array}{ccccc}x_0 & \cdots & x_{M-1} & \cdots & 0\\ \vdots & \iddots & 0 & \iddots & \vdots\\ x_{M-1} & \iddots & & \iddots & 0\\ 0 & \iddots & & \iddots & x_{M-1}\\ \vdots & \iddots & & \iddots & \vdots\\ 0 & \cdots & x_{M-1} & \cdots & x_0\end{array}\right].$$

Now we simply define the Hankel-type matrix of the kind (6)

$$\mathbf{X}_H=\left[\begin{array}{ccccccc}0 & x_1 & \cdots & x_{M-1} & \cdots & 0 & 0\\ \vdots & \vdots & \iddots & 0 & \iddots & \vdots & 0\\ 0 & x_{M-1} & \iddots & & \iddots & 0 & 0\\ 0 & 0 & \iddots & & \iddots & x_{M-1} & 0\\ \vdots & \vdots & \iddots & & \iddots & \vdots & \\ 0 & 0 & \cdots & x_{M-1} & \cdots & x_1 & 0\end{array}\right],$$

which is equal to $\mathbf{X}'_H$ except for its first and last column. Hence

$$\mathbf{X}'_H\cdot[0,\mathbf{b},0]^T=\mathbf{X}_H\cdot[0,\mathbf{b},0]^T,$$

so the matrix $\mathbf{X}_{equiv}=\mathbf{X}_T+\mathbf{X}_H$ performs in the same way that $\boldsymbol{\Upsilon}\cdot\widetilde{\mathbf{X}}$ on vectors of the form $[0,\mathbf{b},0]^T$. Moreover, $\mathbf{X}_{equiv}$ is a sum of two matrices of the kind (5) and (6), so Property 3 of Section III guarantees that it can be perfectly diagonalized via the DCT1e, and the claim holds. By using this result, we finally get

$$\begin{aligned}\mathbf{y}_{\rm m} &= \boldsymbol{\Upsilon}\cdot\mathbf{y}=\boldsymbol{\Upsilon}\cdot\widetilde{\mathbf{X}}\cdot\mathbf{h}_{\rm zp}+\boldsymbol{\Upsilon}\cdot\mathbf{z}\\ &= \mathbf{X}_{equiv}\cdot\mathbf{h}_{\rm zp}+\boldsymbol{\Upsilon}\cdot\mathbf{z},\end{aligned} \tag{13}$$

with the advantage that the whole transform matrix $\mathbf{X}_{equiv}$ is diagonalized by the DCT1e:

$$\mathbf{C}_{1e}\cdot\mathbf{X}_{equiv}\cdot\mathbf{C}_{1e}^{-1}=\mathbf{D}_{\rm (ps)}.$$

Moreover, Property 3 of Section III assures that the diagonal entries of matrix $\mathbf{D}_{\rm (ps)}$ (eigenvalues of $\mathbf{X}_{equiv}$) are the DCT1e transform of the vector $\mathbf{x}_{\rm ZP}^{\rm (r)}=[x_0,\ldots,x_M,0,\ldots,0]^T$, the right-hand side of the pilot symbol (7) zero–padded on the right,

$$d_k^{\rm (ps)}=\left[\mathbf{C}_{1e}\cdot\mathbf{x}_{\rm ZP}^{\rm (r)}\right]_k,\quad k=0,\ldots,N_0-1.$$

Thus, we have been able to find an easy solution to the channel estimation problem by using DCT1e: Let denote $\mathbf{Y}_{\rm m}:=\mathbf{C}_{1e}\cdot\mathbf{y}_{\rm m}$, $\mathbf{H}:=\mathbf{C}_{1e}\cdot\mathbf{h}_{\rm zp}$, and $\mathbf{Z}:=\mathbf{C}_{1e}\cdot\boldsymbol{\Upsilon}\cdot\mathbf{z}$, we get

$$\mathbf{Y}_{\rm m}=\mathbf{D}_{\rm (ps)}\cdot\mathbf{H}+\mathbf{Z}.$$

The coefficients $d_k^{\rm (ps)}$ can be computed and stored in memory when choosing a concrete training signal $\mathbf{x}^{\rm (ps)}$, so they are known. Finally, we obtain an estimation of $\mathbf{H}$,

$$\widehat{\mathbf{H}}_k=[\mathbf{Y}_{\rm m}]_k/d_k^{\rm (ps)},\quad k=0,...,N_0-1 \tag{14}$$

and compute $\mathbf{C}_{1e}^{-1}\cdot\widehat{\mathbf{H}}=\widehat{\mathbf{h}}$ which gives a perfect estimation of $\mathbf{h}_{\rm zp}=[0,\mathbf{h}_{\rm ch}^T,0,...,0]^T$ in absence of noise.

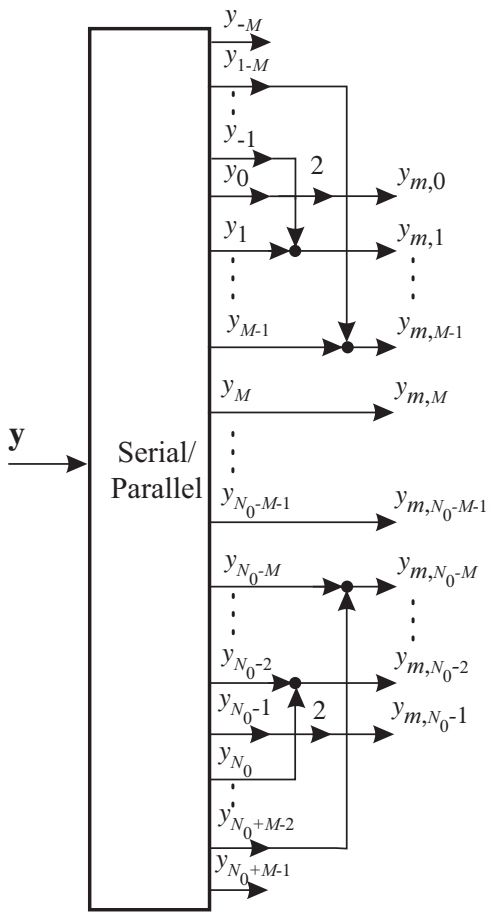

Fig. 3. Mirror, replicate and add (MIRA) block processing at the receiver.

SUMMARY OF THE PROCEDURE:

1) Choose an N_0-length pilot/training signal of the kind $\mathbf{X} = [X_0, 0, X_2, 0, \cdots, X_{N_0-2}]$ and compute $\mathbf{C}_{1e}^{-1} \cdot \mathbf{X} = \mathbf{x}$ which is a WS signal.
2) Compute $\mathbf{d}^{(\mathrm{ps})} = \mathbf{C}_{1e} \cdot \mathbf{x}_{\mathrm{ZP}}^{(\mathrm{r})}$.
3) Transmit $\mathbf{x}^{(\mathrm{ps})}$ through the channel, get the vector $\mathbf{y}$ at the receiver.
4) Modify $\mathbf{y}$ by the MIRA procedure (*mirror* the edge components, *replicate* and *add* to their adjacent ones), so as to get the vector $\mathbf{y}_{\mathrm{m}}$ of length N_0.
5) Apply the DCT1e block: $\mathbf{Y}_{\mathrm{m}} = \mathbf{C}_{1e} \cdot \mathbf{y}_{\mathrm{m}}$.
6) Compute $\widehat{\mathbf{H}}_k = [\mathbf{Y}_{\mathrm{m}}]_k / d_k^{(\mathrm{ps})}$.
7) Finally obtain $\mathbf{C}_{1e}^{-1} \cdot \widehat{\mathbf{H}}$ which is the desired estimation of the zero padded channel filter $[0, \mathbf{h}_{\mathrm{ch}}^T, 0, ..., 0]$.

Notice that it is not necessary to know the length L of the CIR, whenever it is not greater than $N_0 - 2$; but this requirement is fulfilled in practice, where usually the number of subchannels is much greater than the length of the CIR. So our algorithm is able to estimate the channel filter without prior information of its exact or maximum length. This is another important contribution of this work.

Let us finally remark that the computational cost of our procedure is low: on one hand, the DCT1e of N-length vector can be performed in $2N \log_2 N$ operations [28], [29]. On the other hand, the MIRA procedure only implies $2N$ additional sums, so the whole complexity of the proposed MIRA-DCT1e procedure remains of order $2N \log_2 N$. This is another good property of our approach.

B. Validity of the Procedure under Spectral Zeros and Compressed Channel Sensing

Note that Equation (14) cannot be applied in presence of spectral nulls, say, if any of the coefficients $d_k^{(\mathrm{ps})}$ is equal to 0. In other words, if there are spectral nulls, then some of the components $\widehat{\mathbf{H}}_k$ are unknown. Luckily, we show that, even in this case, the proposed scheme is also valid, whenever we know enough components $\widehat{\mathbf{H}}_k$:

Proposition 2: For any set of $L+1$ components $\widehat{\mathbf{H}}_{k_0}, \ldots, \widehat{\mathbf{H}}_{k_L}$ there exists a unique $(L+1)$-length vector $\tilde{\mathbf{h}}$ such that $\widetilde{\mathbf{H}} = \mathbf{C}_{1e} \cdot [\tilde{\mathbf{h}}^T, 0, ..., 0]^T$ verifies $\widetilde{\mathbf{H}}_{k_n} = \widehat{\mathbf{H}}_{k_n}$ for any $n = 0, ..., L$.

Proof: The proof is derived from Property 4 of Section III: let $\mathbf{M}$ be the submatrix of $\mathbf{C}_{1e}$ extracted from its first $(L+1)$ columns, and whose $(L+1)$ rows are the ones indexed as $(k_0, ..., k_L)$; matricially, we have

$$\mathbf{M} \cdot \tilde{\mathbf{h}}^T = [\widehat{\mathbf{H}}_{k_0}, \ldots, \widehat{\mathbf{H}}_{k_L}]^T.$$

Property 4 assures that the $(L+1) \times (L+1)$ matrix $\mathbf{M}$ is invertible, so there exists a unique solution $\tilde{\mathbf{h}}$ which can be perfectly recovered.

Therefore, we can reconstruct the L-length CIR $\mathbf{h}_{\mathrm{ch}}$ whenever there is *any set of* $L+1$ *nonzero coefficients* $d_k^{(\mathrm{ps})}$: In effect, for these $L+1$ indexes k such that $d_k^{(\mathrm{ps})} \neq 0$, we apply Equation (14) and obtain $L+1$ components $\widehat{\mathbf{H}}_k$; then, Proposition 2 guarantees that it suffices to know *any* $L+1$ components of $\widehat{\mathbf{H}}$ in order to perfectly obtain $\tilde{\mathbf{h}} = [0, \mathbf{h}_{\mathrm{ch}}^T]^T$. This result can also be derived from a more general theorem [31], but in the present work we provide a simple and direct proof for DCT1e.

Remark: Thanks to this good property of the DCT1e, we can estimate the channel filter by means of a small number of measurements, so our procedure can also be considered a new technique for Compressed Channel Sensing.

C. Proposed sparse training signal

In this Section we propose a specific training signal which has good properties when using the DCT1e channel estimation scheme proposed in the previous Section. We have used it in our simulations that will be presented in Section VI.

Recalling the properties of the DCT1e obtained in Section III, we easily see that, for odd N_0, the WS signal $[1, 0, 0, 0 \ldots, 0, 1]$ is transformed by DCT1e into the vector

$$[1, 0, 1, 0, \ldots] \sqrt{2/(N_0 - 1)}.$$

In other words, if we choose the original training signal as

$$\mathbf{X} = [1, 0, 1, 0, \ldots]^T$$

then $\mathbf{C}_{1e}^{-1} \cdot \mathbf{X} = \mathbf{x} = [1, 0, 0, \ldots, 0, 1]^T \sqrt{(N_0 - 1)/2}$ which is WS. Its half-right vector, zero padded up to length N_0

is $\mathbf{x}_{\text{ZP}}^{(\text{r})} = \sqrt{(N_0-1)/2}\,[0,\ldots,0,1,0,\ldots,0]^T$. As it has a unique nonzero coefficient which is the central one (at the $n=(N_0-1)/2$ position) then

$$\left[\mathbf{C}_{1e}\cdot\mathbf{x}_{\text{ZP}}^{(\text{r})}\right]_m = \sqrt{\frac{(N_0-1)}{2}}a_{\frac{(N_0-1)}{2}}\cos\left(\frac{m(N_0-1)\pi}{2\,(N_0-1)}\right)$$
$$= \cos\left(m\frac{\pi}{2}\right) = \begin{cases} (-1)^{m/2} \text{ if } m \text{ is even,} \\ 0 \text{ if } m \text{ is odd.}\end{cases}$$

Therefore,

$$\mathbf{d}^{(\text{ps})} = \mathbf{C}_{1e}\cdot\mathbf{x}_{\text{ZP}}^{(\text{r})} = [1,0,-1,0,1,0,-1,0,\ldots]^T$$

and its components are the coefficient $d_k^{(\text{ps})}$. Notice that half of them are null, and the others are alternating $1'$s and $-1'$s.

Thus, when using the training signal as $\mathbf{X}=[1,0,1,0,\ldots]$ with the DCT1e, our channel estimation procedure is very simple. In summary, the estimation has even coefficients of the kind

$$\widehat{\mathbf{H}}_{2k} = [\mathbf{Y}_{\text{m}}]_{2k}\,/d_{2k}^{(\text{ps})} = (-1)^k\,[\mathbf{Y}_{\text{m}}]_{2k},\ 0\le k\le\frac{N_0-1}{2}.$$

Now the remaining question is: *how to estimate the whole filter* $\widehat{\mathbf{h}}$*, if we only know half of the coefficients of its DCT1e transform* $\widehat{\mathbf{H}}$? To answer this question, we provide two methods: On one hand, in the previous section we have guaranteed that the reconstruction is possible whenever at least $L+1$ coefficients $d_k^{(\text{ps})}$ are nonzero (and this is possible if $L\le(N_0-1)/2$). On the other hand, we give another method by recalling Properties 1 and 2: if we set all odd components equal to 0,

$$\widehat{\mathbf{H}}_{2k-1}=0,\quad k=1,\ldots,(N_0-1)/2.$$

Then we have a vector of the kind $\widehat{\mathbf{H}}=[\widehat{H}_0,0,\widehat{H}_2,0,...]^T$ which has odd null components, so by (3), $\widehat{\mathbf{h}}=\mathbf{C}_{1e}\cdot\widehat{\mathbf{H}}$ is a WS vector that, in absence of noise, can be written as

$$\widehat{\mathbf{h}} = (\mathbf{h}_{\text{zp}}+\mathbf{J}\cdot\mathbf{h}_{\text{zp}})/2.$$

Moreover, if $L\le(N_0-3)/2$ (condition usually met in practice), then we obtain the following expression:

$$\widehat{\mathbf{h}} = [0,\mathbf{h}_{\text{ch}}^T,0,...,0,\ (\mathbf{J}\cdot\mathbf{h}_{\text{ch}})^T,\ 0]^T/2.$$

This way, the vector that appears in the first half is the CIR $\mathbf{h}_{\text{ch}}$, whereas in the right half we find its mirror version $\mathbf{J}\cdot\mathbf{h}_{\text{ch}}$, with eventual zeros appended at both edges, and a factor of $1/2$.

V. Signal Reconstruction via DCT1e

Let us suppose we have already estimated the channel and, if necessary, it has been symmetrized by means of a pre-filter[2]. So, we can consider the impulse response of the channel as

$$\mathbf{h}=[h_{L-1},\ldots,h_1,\,h_0,\,h_1,\ldots,h_{L-1}].$$

Now the problem is to recover the data symbol $\mathbf{X}$ at the receiver as in Figure 1. Now the transmitted data needs to be of even length, so N is supposed to be $N=N_0+1$. In a previous work [25] the DCT1e was applied for single-carrier modulation; there, the problem was addressed by appending at least $L-1$ redundant data as prefix and also $L-1$ samples as suffix to the each data symbol, by enforcing a WS symmetry. As a result, each transmitted data could be reconstructed at the receiver.

In this section we propose a new and simple approach with zero padding and that avoids the use of symmetric extension. The key idea is that the commutative property of the convolution product allows us to interchange the roles of the signal and the channel. By using the MIRA procedure, it will be able to reconstruct an arbitrary signal of even length, just by using $N-2$ subchannels for data, and enforcing the remaining 2 at each edge with a predetermined value obtained from the rest of data, as we explain next.

The transmitted data vector in the transform domain is $\mathbf{X}=[X_0,X_1,\ldots,X_{N-2},X_{N-1}]$. Based on Proposition 1, we are able to transmit the time-domain information data without using symmetric extension provided that the vector $\mathbf{x}$ is of the form $\mathbf{x}=[0,\mathbf{x}_c^T,0]^T$. As $\mathbf{x}=\mathbf{C}_{1e}^{-1}\cdot\mathbf{X}$ (see Figure 1), we must choose X_0 and X_{N-1} such that the first and last components of $\mathbf{C}_{1e}^{-1}\cdot\mathbf{X}$ are null. Taking into account first and last rows of $\mathbf{C}_{1e}^{-1}$ (for N even) are respectively proportional to

$$\left[\begin{array}{ccccccccc} 1 & 2 & 2 & \ldots & 2 & 2 & 1 \end{array}\right],$$
$$\left[\begin{array}{ccccccccc} 1 & -2 & 2 & \ldots & -2 & 2 & -1 \end{array}\right],$$

the equations that must be fulfilled are

$$X_0+2\sum_{j=1}^{N-2}X_j+X_{N-1}=0,$$
$$X_0-2\sum_{j=1}^{N-2}(-1)^jX_j-X_{N-1}=0.$$

Adding and subtracting these two equations, one gets the the conditions that must be satisfied by the first and the last components of vector $\mathbf{X}$:

$$X_0=-2\sum_{j=1}^{N/2-1}X_{2j-1}, \tag{15a}$$
$$X_{N-1}=-2\sum_{j=1}^{N/2-1}X_{2j}. \tag{15b}$$

The central part of the received vector,

$$\widetilde{\mathbf{y}}=\mathbf{h}*\mathbf{x}+\mathbf{z},$$

has length $N+2L$ and may be written as

$$\widetilde{\mathbf{y}}=\mathbf{H}\cdot\mathbf{x}+\mathbf{z},$$

which corresponds to (8), by changing the roles of signal and CIR. The transmission matrix, $\mathbf{H}$, of size $(N+2L)\times N$, is Toeplitz with first row $[h_{L-1},\,0,\,\ldots,\,0]$ and first column $[\mathbf{h}^T,\,0,\,\ldots,\,0]^T$. This matrix $\mathbf{H}$ can be folded by using the MIRA procedure described on Figure 3, i e., multiplying it by $\boldsymbol{\Upsilon}$, defined in (12) with dimensions $N\times(N+2L)$. As a result, we get an $N\times N$ matrix $\mathbf{H}_{equiv}$ which is diagonalizable by the DCT1e.

[2]It can be easily implemented using $\mathbf{h}_{\text{pf}}=\mathbf{J}\cdot\widehat{\mathbf{h}}$.

As shown in the lower part of Figure 1, the modified received vector is given by

$$\widetilde{\mathbf{y}}_{\mathrm{r}} = \boldsymbol{\Upsilon} \cdot \widetilde{\mathbf{y}} = \mathbf{H}_{equiv} \cdot \mathbf{x} + \widetilde{\mathbf{z}}, \tag{16}$$

where $\mathbf{H}_{equiv} = \mathbf{C}_{1e}^{-1} \cdot \widetilde{\mathbf{D}} \cdot \mathbf{C}_{1e}$, being $\widetilde{\mathbf{D}}$ a diagonal matrix. Now, we apply the DCT1e to both sides of (16):

$$\mathbf{C}_{1e} \cdot \widetilde{\mathbf{y}}_{\mathrm{r}} = \mathbf{C}_{1e} \cdot \mathbf{H}_{equiv} \cdot \mathbf{x} + \mathbf{C}_{1e} \cdot \tilde{\mathbf{z}}.$$

By denoting $\widetilde{\mathbf{Y}}_{\mathrm{r}} = \mathbf{C}_{1e} \cdot \widetilde{\mathbf{y}}_{\mathrm{r}}$, $\widetilde{\mathbf{Z}} = \mathbf{C}_{1e} \cdot \tilde{\mathbf{z}}$, and noting that $\mathbf{C}_{1e} \cdot \mathbf{H}_{equiv} = \widetilde{\mathbf{D}} \cdot \mathbf{C}_{1e}$, we have

$$\widetilde{\mathbf{Y}}_{\mathrm{r}} = \widetilde{\mathbf{D}} \cdot \mathbf{C}_{1e} \cdot \mathbf{x} + \widetilde{\mathbf{Z}}. \tag{17}$$

It suffices to recall $\mathbf{X} = \mathbf{C}_{1e} \cdot \mathbf{x}$, and we finally express (17) as

$$\widetilde{\mathbf{Y}}_{\mathrm{r}} = \widetilde{\mathbf{D}} \cdot \mathbf{X} + \widetilde{\mathbf{Z}}.$$

Thus, we obtain an estimate of the extended vector as:

$$\hat{\mathbf{X}} = \widetilde{\mathbf{D}}^{-1} \cdot \widetilde{\mathbf{Y}}_{\mathrm{r}} - \widetilde{\mathbf{D}}^{-1} \cdot \widetilde{\mathbf{Z}}, \tag{18}$$

where the entries of the diagonal matrix $\widetilde{\mathbf{D}}$ are the components of

$$\mathbf{C}_{1e} \cdot [h_0,\, h_1, \ldots, h_{L-1}, 0, \ldots, 0]^T.$$

By discarding both the first and last components in (18) we obtain the reconstructed data $\widehat{\mathbf{X}}_i = [\hat{X}_1, \ldots, \hat{X}_{N-2}]$. Therefore, in the absence of noise, the central components of $\widehat{\mathbf{X}} = \widetilde{\mathbf{D}}^{-1} \cdot \widetilde{\mathbf{Y}}_{\mathbf{r}}$ provide a perfect reconstruction of the information vector $\mathbf{X}_i = [X_1, \ldots, X_{N-2}]$ without using any symmetric extension. The performance of the method in the noisy case is also excellent, as shown in Section VI.

VI. Numerical Results

In this section, we analyse the behaviour of the proposed transceiver, both in terms of channel estimation and signal reconstruction, by testing it on several channels. First of all, in Section VI-A we test it on a fixed channel of length $L = 11$. Then, in Section VI-B we test it on several standardized ITU-R M.1225 channels [32].

In order to test the **channel estimation**, a sparse signal is constructed in the DCT1e domain by setting $X_k = 1$ if $k = rK$ (for some given value of K, which acts as a sparsity parameter for the transmitted signal in the DCT1e domain) and $X_k = 0$ otherwise. The inverse DCT1e is performed and the extended time-domain transmitted signal ($\mathbf{x}_e$) is passed through the filter with impulse response $\mathbf{h}_{\mathrm{ch}}$. Then, zero-mean additive white Gaussian noise (AWGN) with variance σ_z^2 is added, resulting in a received signal whose central part is $\mathbf{y} = \mathbf{x} * \mathbf{h}_{\mathrm{ch}} + \mathbf{z}$, where $z_n \sim \mathcal{N}(0, \sigma_z^2)$ with $\mathcal{N}(\mu, \sigma^2)$ denoting a univariate Gaussian density with mean μ and variance σ^2. The MIRA process is applied on the length $L + N - 1$ sequence $\mathbf{y}$, resulting in a length $N = N_0$ sequence $\mathbf{y}_{\mathrm{m}}$. The N-th order DCT1e of $\mathbf{y}_{\mathrm{m}}$ ($\mathbf{Y}_m$) is computed and then it is used to estimate the DCT1e of the channel's impulse response ($\widehat{H}_k$) as indicated in the text. Note that only one out of P ($P = 2$ or $P = 4$) coefficients is reconstructed. Finally, the length N inverse DCT1e of $\widehat{H}_k$ is obtained and the relevant central samples are extracted to obtain the estimate of the channel's impulse response, $\hat{\mathbf{h}}$. The performance measure used is the normalized mean squared error (NMSE) in the reconstruction of the CIR:

$$\mathrm{NMSE(dB)} = 10 \log_{10} \frac{P_e}{P_h},$$

with $P_e = \frac{1}{L}(\mathbf{h}_{\mathrm{ch}} - \hat{\mathbf{h}})^T(\mathbf{h}_{\mathrm{ch}} - \hat{\mathbf{h}}) = \frac{1}{L}\sum_{n=0}^{L-1} |h_{\mathrm{ch}}(n) - \hat{h}(n)|^2$, $P_h = \frac{1}{L}\mathbf{h}_{\mathrm{ch}}^T\mathbf{h}_{\mathrm{ch}} = \frac{1}{L}\sum_{n=0}^{L-1} |h_{\mathrm{ch}}(n)|^2$ and L denoting the CIR's length. All of the system's parameters (the transmitted signal power to noise ratio, the length of the DCT1e, the number of pilot subcarriers used in the transmitter and the number of reconstruction coefficients used in the receiver) are changed in order to see their effect in the quality of the estimated channel's impulse response. In our simulations, we make the reasonable assumption that the errors due to channel estimation and time variation are uncorrelated; the channel is relatively stationary over the short duration of the training symbol. We consider that channel estimation is developed under the assumption of slow fading channel, where the channel is assumed to be constant within a frame, but varies from frame to frame. Hence, one pilot symbol should be inserted at the beginning of each frame to estimate the channel, as shown in Figure 2.

For the **signal reconstruction**, we generate a sequence of $N - 2$ (with even $N = N_0 + 1$) independent binary symbols $[X_1, \ldots, X_{N-2}]$, constructing X_0 and X_{N-1} as described in Section V. The inverse DCT1e is performed and the extended time-domain transmitted signal ($\mathbf{x}_e$) is passed through the global channel's impulse response, $\mathbf{h} = \mathbf{h}_{\mathrm{ch}} * \mathbf{h}_{\mathrm{pf}}$. Both the ideal pre-filter (which corresponds to the time-reversed CIR $\mathbf{h}_{\mathrm{ch}}$) and the estimated pre-filter (constructed from the estimated $\hat{\mathbf{h}}$) are considered. In the receiver, MIRA is applied on the length $2L+N-2$ signal $\widetilde{\mathbf{y}}$ in order to obtain a length N sequence $\widetilde{\mathbf{y}}_{\mathrm{r}}$. The DCT1e of this sequence is performed, and the stored channel equalization coefficients used to recover the transmitted information. The performance measure in this case is the bit error rate (BER),

$$\mathrm{BER} = \frac{1}{N N_s} \sum_{i=1}^{N_s} \sum_{k=1}^{N-2} [\![\hat{X}_k^{(i)} \neq X_k^{(i)}]\!], \tag{19}$$

where N_s is the number of MCM symbols used in the simulations, and $[\![\mathcal{LC}]\!] = 1$ if the logical condition $\mathcal{LC}$ is fulfilled and $[\![\mathcal{LC}]\!] = 0$ otherwise.

A. Fixed Channel

As a first example, we select the following $L = 11$ sparse channel that has only 4 non-null coefficients: $\mathbf{h} = [1, 0, 0, -0.5, 0, 0, 0, 0.25, 0, 0, 0.05]^T$. In this case, we set the length of the DCT1e to $N = N_0 = 511$ and check the behaviour of the channel estimation and signal reconstruction schemes as the SNR increases (from -10 dB to 30 dB) for a varying number of pilot subcarriers in the transmitter (from $N_p = 2$ to $N_p = 256$) and reconstruction coefficients in the receiver (128 or 256). $N_s = 2000$ simulations (i.e., MCM symbols) are used for each case.

1) Channel Estimation: Figure 4 shows three examples of the estimated channel's impulse and frequency responses for three signal to noise ratios (SNR = 0 dB, SNR = 10 dB and SNR = 20 dB) using $N_p = 256$ pilot subcarriers in the transmitter and 256 reconstruction coefficients in the receiver. The channel's impulse response is displayed on the top row (central dot with the true values and bar spanning the range from the minimum to the maximum recovered values), whereas the bottom row shows the channel's frequency response (true value in black line and shaded area showing the range from the maximum to the minimum values). Note the substantial decrease in the variation of the coefficients of the channel's impulse response as the SNR increases (indeed, for SNR = 20 dB the bars cannot be appreciated, since the recovered coefficients are always virtually identical to the true coefficients) and the corresponding improvement in the estimation of the channel's frequency response (with a substantial decrease in the shaded area).

Figure 5 shows the effect, on the recovered channel's frequency response, of changing the number of subcarriers in the transmitter and the reconstruction coefficients in the receiver. In all cases an SNR = 20 dB is used and $N_s = 2000$ simulations are performed again, and we compare the quality of the recovered $\widehat{H}(\omega)$ using $N_p = 127$ (Figs. 5(a)&(d)), $N_p = 17$ (Figs. 5(b)&(e)) and $N_p = 3$ (Figs. 5(c)&(f)). For figures on the top row 256 coefficients are used to reconstruct the channel in the receiver, whereas only 128 coefficients are used for figures on the bottom row. First of all, let us remark that using only 128 coefficients does not degrade substantially the performance of the proposed approach. Note also that the performance decreases as less subcarriers are used (using 256 coefficients in the receiver, the NMSE increases from -69.81 dB for $N_p = 129$ to -25.34 dB for $N_p = 3$).

TABLE I
SNR GAIN IN THE ESTIMATION OF THE CHANNEL FOR $N = N_0 = 511$. K: SPARSITY PARAMETER FOR THE DCT1E OF THE TRANSMITTED SIGNAL; $N_p = (N+1)/K$: TOTAL NUMBER OF PILOT SUBCARRIERS USED IN THE TRANSMITTER (IN PARENTHESIS THE TOTAL NUMBER OF PILOTS USING AN ADDITIONAL CENTRAL PILOT, $N_p = (N+1)/K + 1$); P: SPARSITY PARAMETER FOR THE RECONSTRUCTION OF THE SIGNAL; N_r: NUMBER OF COEFFICIENTS USED TO RECONSTRUCT THE CHANNEL IN THE RECEIVER ($N_r = (N+1)/P$); ΔSNR(DB): SNR GAIN IN EQ. (20) (IN PARENTHESIS THE GAIN USING THE ADDITIONAL CENTRAL PILOT).

K	N_p	P	N_r	ΔSNR(dB)
2	256	2	256	15.05
4	128 (129)	2	256	10.25 (10.30)
		4	128	8.08 (8.09)
8	64 (65)	2	256	6.55 (6.62)
		4	128	4.59 (4.64)
16	32 (33)	2	256	3.16 (3.31)
		4	128	1.31 (1.43)
32	16 (17)	2	256	-0.14 (0.14)
		4	128	-1.93 (-1.68)
64	8 (9)	2	256	-3.49 (-2.90)
		4	128	-5.27 (-4.73)
128	4 (5)	2	256	-7.20 (-5.94)
		4	128	-8.98 (-7.74)
256	2 (3)	2	256	-11.99 (-8.97)
		4	128	-13.75 (-10.77)

However, an accurate estimation of the channel can be provided, if the SNR is large enough, even when only $N_p = 3$ pilot subcarriers are used. This is shown in Figure 6, where the performance as a function of the SNR is shown for different values of N_p and N_r. In all cases the NMSE(dB) decreases linearly (i.e., the $-$NMSE(dB) shown in Figure 6 increases linearly) as the signal power to noise ratio increases. Indeed, the following relationship can be established:

$$-\text{NMSE(dB)} = \text{SNR(dB)} + \Delta\text{SNR(dB)}, \qquad (20)$$

where $\text{SNR(dB)} = 10\log_{10}\frac{P_x}{\sigma_z^2}$ with $P_x = \frac{1}{N}\mathbf{x}^T\mathbf{x} = \frac{1}{N}\sum_{n=0}^{N-1}|x(n)|^2$, and $\Delta\text{SNR(dB)}$ is given in Table I. Note that there is a large difference in performance between the best case ($N_p = 256$ and $N_r = 256$) and the worst case ($N_p = 2$ and $N_r = 128$), but in all cases a fixed NMSE can be attained if the signal power to noise ratio is large enough. For instance, if NMSE $= -40$ dB is sought, this can be achieved using only SNR $= 24.95$ dB in the best case ($N_p = 256$ and $N_r = 256$), but it can also be achieved in the worst case ($N_p = 2$ and $N_r = 128$) if we have SNR $= 53.75$ dB. Hence, the sparsest transmission/reconstruction scheme can be applied when the noise is low enough. Figure 6 also shows the NMSE attained when the DFT is used to estimate the channel in the receiver. Once more, the linear relationship given in (20) among the $-$NMSE(dB) and the SNR(dB) is obtained, but ΔSNR $= -1.60$ dB now (i.e., similar to the ΔSNR(dB) obtained using our proposed approach with $K = 32$ and $P = 4$ shown in Table I). This shows that, using the MIRA-based procedure proposed in this paper, we can achieve a much better performance in terms of channel estimation than other DCT-MCM methods which use the DFT to estimate the channel (e.g., [16]–[19]).

2) Signal Reconstruction: In order to test the signal reconstruction capability of the proposed approach (i.e., its ability to recover the transmitted information symbols), we consider again the fixed channel with CIR $\mathbf{h}_{\text{ch}} = [1, 0, 0, -0.5, 0, 0, 0, 0.25, 0, 0, 0.05]^T$. We test the BER using a variable order of the DCT1e, $N = N_0 + 1 \in \{128, 256, 512, 1024, 2048\}$, and two modulation schemes in the subcarriers: binary phase shift keying (BPSK) and 64 quadrature amplitude modulation (64-QAM). Figure 7 shows the BER, as a function of the SNR (using a range from -10 dB to 40 dB with a step of 1 dB), for $N = 128$. The performance obtained using the true channel's impulse response (in blue dotted line) to construct the prefilter is compared to the performance obtained using the estimated CIR (in red solid line) using the procedure described in Section V. The performance using the DFT to estimate the CIR and construct the prefilter is also included (in green dashed line). For each SNR, $N_s = 100$ simulations are performed, transmitting $N_b = 1000$ blocks (i.e., MCM symbols) through the channel in each case. This results in a total number of transmitted BPSK/64-QAM symbols equal to $10^5 \times (N-2)$ for each SNR to estimate the BER. From Figure 7(a), it can be seen that the performance of the realistic system (i.e., the one which uses the estimated CIR) is almost identical to that of the ideal system (which assumes the CIR known and uses it to construct the prefilter) when using the BPSK modulation in the subcarriers (e.g., an SNR $= 32.4$ dB is required in both

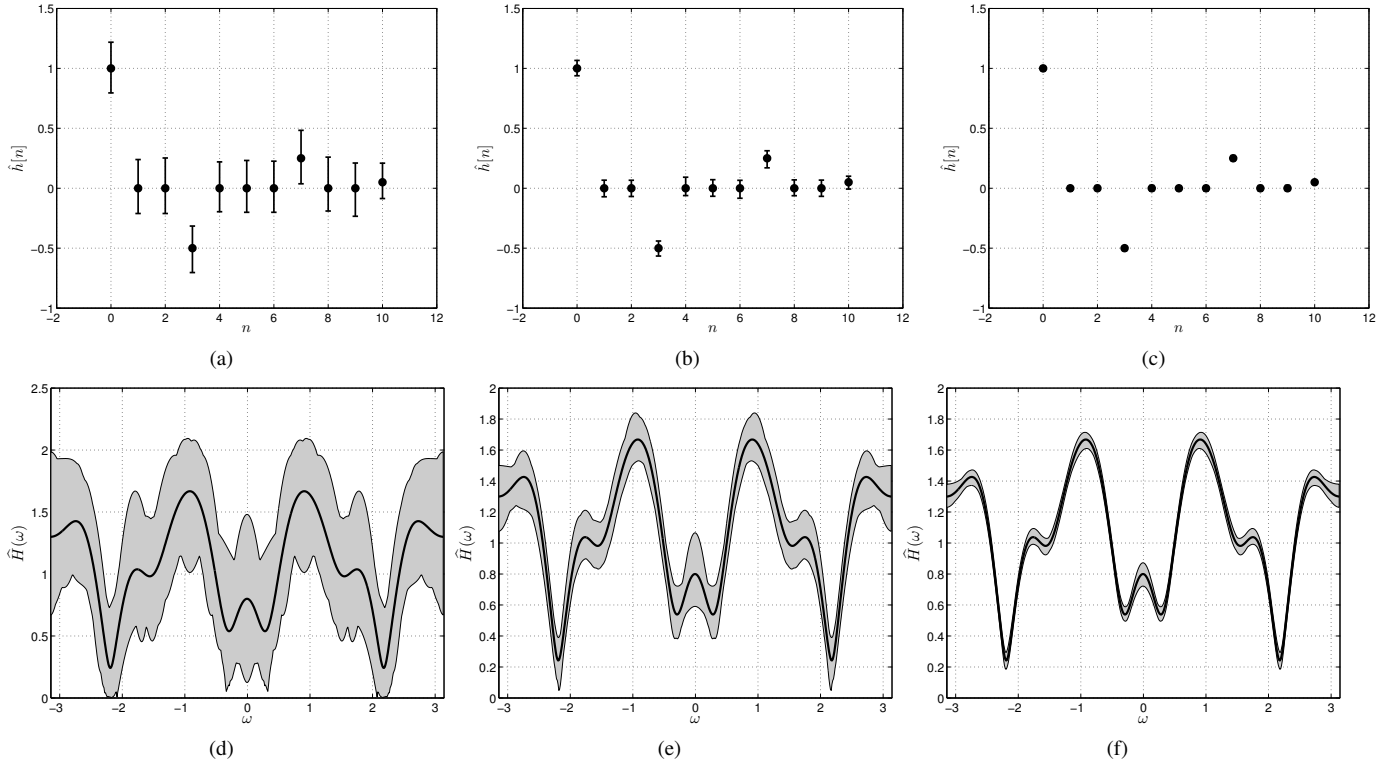

Fig. 4. (a)–(c): Estimated channel's impulse response: (a) SNR = 0 dB, (b) SNR = 10 dB, and (c) SNR = 20 dB. (d)–(f): Estimated channel's frequency response: (a) SNR = 0 dB, (b) SNR = 10 dB, and (c) SNR = 20 dB. In all cases the length of the DCT1e is $N = N_0 = 511$, $N_p = 256$ pilot subcarriers are used in the transmitter and $N_r = 256$ reconstruction coefficients are used in the receiver.

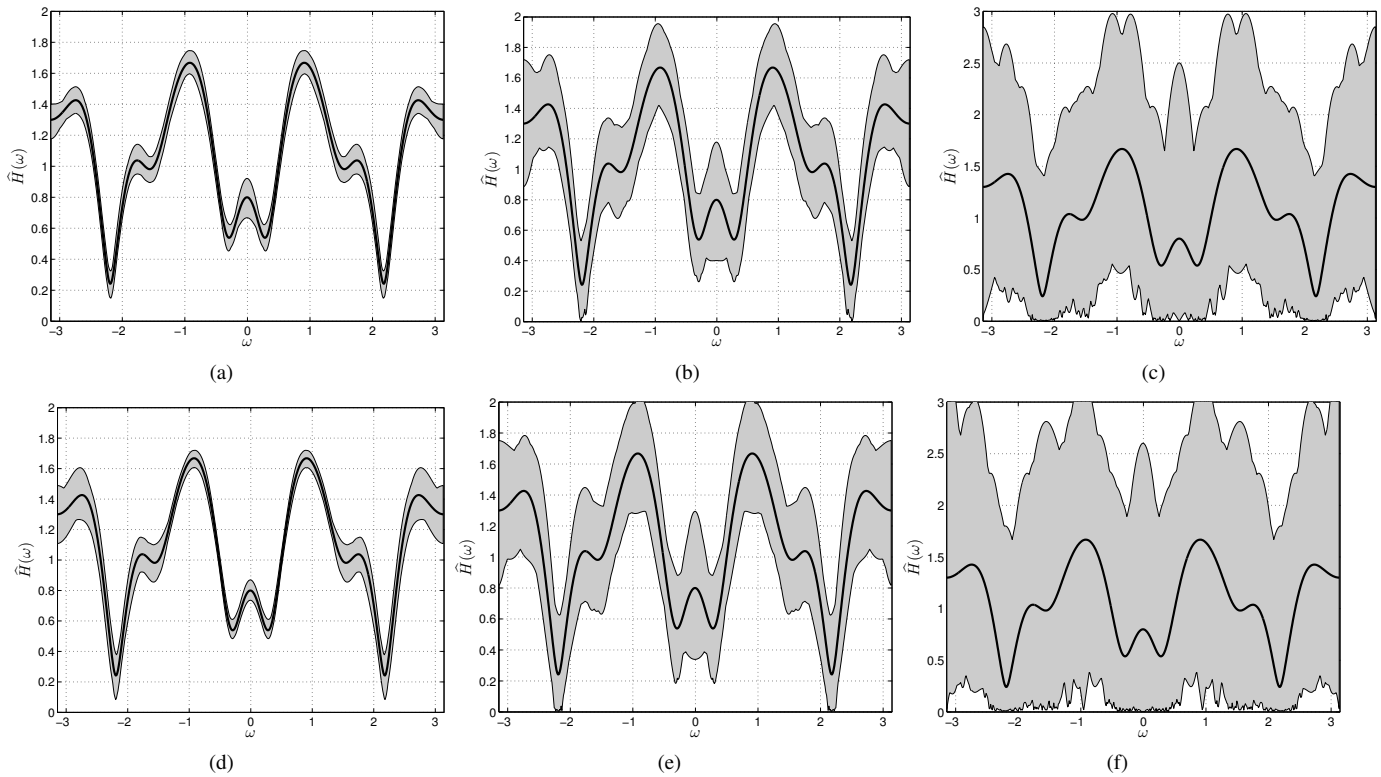

Fig. 5. Estimated channel's frequency response for an order $N = N_0 = 511$ DCT1e and SNR = 20 dB. (a) & (d): $K = 4$ with a central pilot ($N_p = 129$ pilot subcarriers overall) using 256 and 128 reconstruction coefficients respectively. (b) & (e): $K = 32$ with a central pilot ($N_p = 17$ pilot subcarriers overall) using 256 and 128 reconstruction coefficients respectively. (c) & (f): $K = 256$ with a central pilot ($N_p = 3$ pilot subcarriers overall) using 256 and 128 reconstruction coefficients respectively.

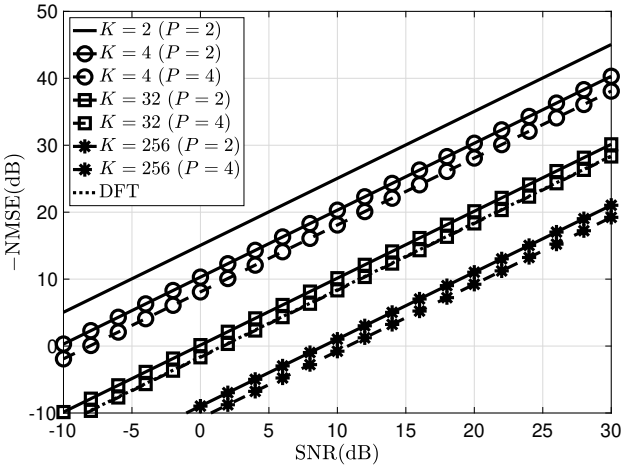

Fig. 6. Normalised mean squared error (NMSE(dB)) as a function of the signal power to noise ratio (SNR(dB)) for different values of K (sparsity parameter for the DCT1e of the transmitted signal) and P (sparsity parameter for the reconstruction). The NMSE using the DFT to estimate the channel is also shown. In all cases, the length of the DCT1e is $N = N_0 = 511$ and $N_s = 2000$ simulations have been performed. Note that $-$NMSE(dB) is actually plotted in the figure, so higher values correspond to a better performance.

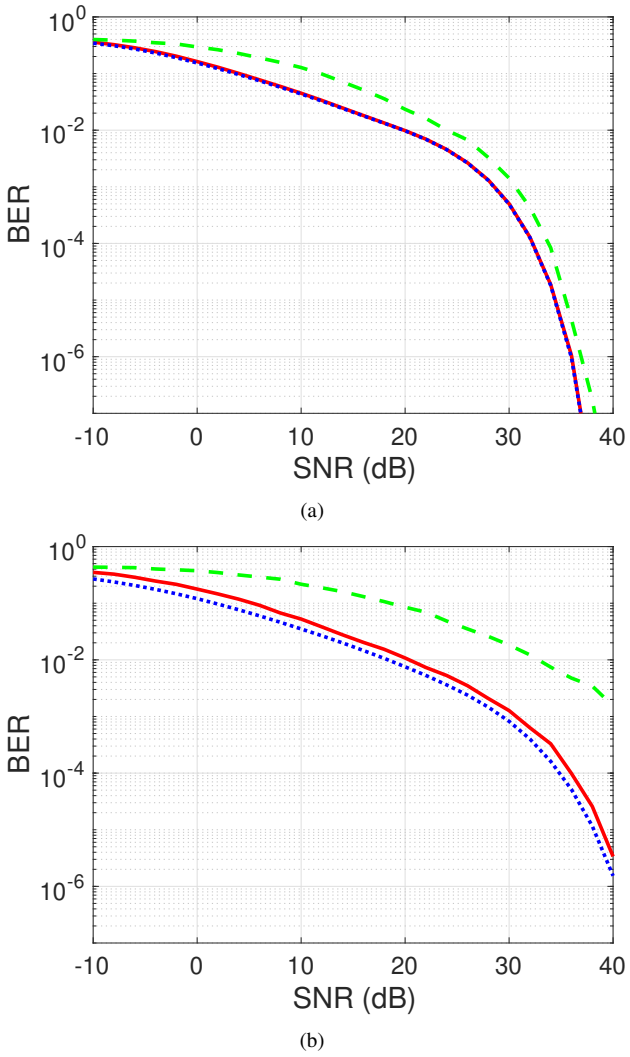

Fig. 7. Comparison of the BER attained using the ideal known channel to construct the prefilter (dotted blue line) the estimated channel using the MIRA procedure proposed in the paper (solid red line) and the DFT as in [16]–[19] (dashed green line), for the fixed channel with CIR $\mathbf{h} = [1, 0, 0, -0.5, 0, 0, 0, 0.25, 0, 0, 0.05]^T$, using an order $N = 256$ DCT1e. (a) Using BPSK modulation in the subcarriers. (b) Using 64-QAM in the subcarriers.

cases to attain a BER $= 10^{-4}$). However, there is a substantial loss in performance when the CIR is estimated using the DFT in the receiver. When 64-QAM is used in the subcarriers, the performance degrades as expected (e.g., an SNR $= 36.4$ dB is required in the ideal case for a BER $= 10^{-4}$) and the distance between the ideal and the realistic systems increases (e.g., an SNR $= 37.8$ dB is required for a BER $= 10^{-4}$), as the 64-QAM demodulator is more sensitive to errors in the CIR's estimation, but a good performance is still attained. Using the DFT to estimate the CIR results in a larger difference w.r.t. the ideal system and a substantial loss in the system's performance. The situation is similar for all the other values of N. Indeed, as the value of N increases the difference becomes smaller and smaller, as shown in Table II and Table III for a BPSK and 64-QAM in the subcarriers, respectively. This confirms the good performance of the channel estimation procedure and the robustness of the proposed approach w.r.t. errors in the construction of the prefilter.

B. ITU-R M.1225 Channels

1) Channel Estimation: As a second example, we consider several of the channels standardized by ITU-R for the evaluation of radio transmission technologies for IMT 2000 [32]. Table IV shows the SNR gain, ΔSNR(dB), in the estimation of the ITU-R M.1225 pedestrian channel A for an increasing length of the DCT1e (from $N = 127$ to $N = 1023$) and different values for the total number of pilot subcarriers used in the transmitter. In all cases, $N_s = 2000$ simulations were performed for an SNR ranging from -10 dB to 30 dB and $N_r = 256$ coefficients were used for the reconstruction in the receiver. The channel was generated using Matlab's `stdchan` function using a carrier frequency $f_c = 2$ GHz and a sampling period $T_s = 10$ ns. The resulting channel's impulse response has length $L = 42$ but only 4 non-null coefficients located at $n \in \{0, 11, 19, 41\}$ with amplitudes following a Rayleigh distribution. Therefore, given the high sparsity of the channel (less than 10% non-null coefficients), comparing Table I and Table IV we can see that the results are even better than for the shorter channel considered in the previous section. Figure 8 shows the NMSE(dB) as a function of the signal power to noise ratio (SNR(dB)), both for different values of N and N_p, comparing it to the the NMSE(dB) obtained using the scheme proposed in [21]. Note the large increase in the attained NMSE(dB) (up to 15 dB when $N = 127$) for a given SNR(dB) in all cases.

The same experiment ($f_c = 2$ GHz, $T_s = 10$ ns, $N_s = 2000$ simulations, $N_r = 256$ coefficients and $N \in \{127, 255, 511, 1023\}$) has been performed for two other ITU-R M.1225 channels: indoor office channel A ($L = 32$, 6 non-null coefficients) and indoor office channel B ($L = 71$, 6 non-null coefficients). The results (not shown) are almost

TABLE II

ESTIMATED BER AS A FUNCTION OF THE SNR (DB) AND THE ORDER OF THE DCT1E USED (N) FOR THE FIXED CHANNEL WITH CIR $\mathbf{h} = [1, 0, 0, -0.5, 0, 0, 0, 0.25, 0, 0, 0.05]^T$ USING BPSK MODULATION IN THE SUBCARRIERS. IN EACH COLUMN, THE FIRST RESULT CORRESPONDS TO ASSUMING A KNOWN CHANNEL AND THE SECOND ONE (IN PARENTHESES) TO THE ESTIMATED CHANNEL.

SNR (dB)	128	256	512	1024	2048
0	0.1539 (0.1731)	0.1536 (0.1601)	0.1534 (0.1578)	0.1533 (0.1561)	0.1533 (0.1538)
5	0.0848 (0.0942)	0.0845 (0.0883)	0.0844 (0.0866)	0.0843 (0.0857)	0.0843 (0.0848)
10	0.0435 (0.0460)	0.0435 (0.0446)	0.0435 (0.0440)	0.0435 (0.0436)	0.0434 (0.0436)
15	0.0206 (0.0219)	0.0208 (0.0214)	0.0208 (0.0209)	0.0208 (0.0208)	0.0208 (0.0209)
20	$9.71\ (9.97) \times 10^{-3}$	$9.73\ (9.89) \times 10^{-3}$	$9.77\ (9.73) \times 10^{-3}$	$9.78\ (9.86) \times 10^{-3}$	$9.78\ (9.76) \times 10^{-3}$
25	$3.49\ (3.57) \times 10^{-3}$	$3.53\ (3.56) \times 10^{-3}$	$3.52\ (3.52) \times 10^{-3}$	$3.52\ (3.51) \times 10^{-3}$	$3.53\ (3.53) \times 10^{-3}$
30	$4.96\ (5.21) \times 10^{-4}$	$4.90\ (5.05) \times 10^{-4}$	$4.88\ (4.93) \times 10^{-4}$	$4.95\ (4.99) \times 10^{-4}$	$4.97\ (5.00) \times 10^{-4}$
35	$5.20\ (5.28) \times 10^{-5}$	$4.40\ (4.63) \times 10^{-5}$	$5.64\ (5.70) \times 10^{-5}$	$4.59\ (4.61) \times 10^{-5}$	$4.87\ (4.80) \times 10^{-5}$

TABLE III

ESTIMATED BER AS A FUNCTION OF THE SNR (DB) AND THE ORDER OF THE DCT1E USED (N) FOR THE FIXED CHANNEL WITH CIR $\mathbf{h} = [1, 0, 0, -0.5, 0, 0, 0, 0.25, 0, 0, 0.05]^T$ USING 64-QAM IN THE SUBCARRIERS. IN EACH COLUMN, THE FIRST RESULT CORRESPONDS TO ASSUMING A KNOWN CHANNEL AND THE SECOND ONE (IN PARENTHESES) TO THE ESTIMATED CHANNEL.

SNR (dB)	128	256	512	1024	2048
0	0.1372 (0.2197)	0.1203 (0.1832)	0.1076 (0.1452)	0.0992 (0.1213)	0.0958 (0.1058)
5	0.0798 (0.1325)	0.0676 (0.0997)	0.0589 (0.0782)	0.0536 (0.0640)	0.0514 (0.0564)
10	0.0421 (0.0683)	0.0351 (0.0522)	0.0302 (0.0388)	0.0271 (0.0319)	0.0258 (0.0281)
15	0.0209 (0.0346)	0.0171 (0.0243)	0.0144 (0.0182)	0.0127 (0.0150)	0.0119 (0.0128)
20	$9.45\ (14.62) \times 10^{-3}$	$7.54\ (10.50) \times 10^{-3}$	$6.20\ (7.69) \times 10^{-3}$	$5.38\ (6.15) \times 10^{-3}$	$4.99\ (5.46) \times 10^{-3}$
25	$3.85\ (6.20) \times 10^{-3}$	$2.95\ (4.53) \times 10^{-3}$	$2.30\ (3.06) \times 10^{-3}$	$1.89\ (2.23) \times 10^{-3}$	$1.65\ (1.81) \times 10^{-3}$
30	$1.22\ (2.10) \times 10^{-3}$	$0.82\ (1.32) \times 10^{-3}$	$0.54\ (0.77) \times 10^{-3}$	$0.37\ (0.46) \times 10^{-3}$	$0.27\ (0.32) \times 10^{-3}$
35	$2.03\ (4.53) \times 10^{-4}$	$0.95\ (1.76) \times 10^{-4}$	$0.42\ (0.66) \times 10^{-4}$	$0.18\ (0.25) \times 10^{-4}$	$0.08\ (0.11) \times 10^{-4}$

TABLE IV

SNR GAIN IN THE ESTIMATION OF THE CHANNEL FOR THE ITU-R M.1225 PEDESTRIAN CHANNEL A. $N_p = (N+1)/K$: TOTAL NUMBER OF PILOT SUBCARRIERS IN THE TRANSMITTER; N: TOTAL NUMBER OF SUBCARRIERS; ΔSNR(DB): SNR GAIN IN EQ. (20).

K	ΔSNR(dB)			
	$N = 127$	$N = 255$	$N = 511$	$N = 1023$
2	18.02	21.05	24.08	27.09
4	12.96	15.86	18.87	21.83
8	9.38	12.31	15.29	18.29
16	6.19	9.14	12.12	15.12
32	3.14	6.09	9.07	12.06
64	0.11	3.07	6.04	9.05

identical to those in Table IV. Finally, a similar experiment has also been performed for two much longer channels: pedestrian channel B ($L = 371$, 6 non-null coefficients) and vehicular channel A ($L = 252$, 6 non-null coefficients). Once more, the results (not shown) are almost identical to those in Table IV for those cases where $N > 2L - 1$ ($N = 1023$ in the first case; $N = 511$ and $N = 1023$ in the second case). This confirms the good performance of the proposed scheme, regardless of the length of the channel's impulse response, as long as $N > 2L - 1$.

2) Signal Reconstruction: Once more, we consider the pedestrian channel A of ITU-R M.1225 with $f_c = 2$ GHz and $T_s = 10$ ns. We test again the BER using a variable order of the DCT1e, $N \in \{128, 256, 512, 1024, 2048\}$, and a BPSK modulation in the subcarriers. Figure 9 shows the BER, as a function of the SNR, for $N = 128$, $N = 512$ and $N = 2048$. The performance obtained using the true channel's impulse response (in blue dotted line) to construct the prefilter is compared to the performance obtained using the estimated CIR (in red solid line) using the procedure described in Section V. For each SNR, $N_b = 1000$ blocks (i.e., MCM symbols) are transmitted through each of the $N_c = 100$ randomly generated channels according to the ITU-R M.1225 model. This results in a total number of transmitted BPSK symbols equal to $10^5 \times (N - 2)$ for each SNR to estimate the BER.

From Figure 9, it can be seen that there is a small gap in the performance of the realistic system w.r.t. the ideal system, but this gap decreases as N increases and both curves become virtually identical for $N = 2048$. This situation can be appreciated more clearly in Table V, where the numerical values corresponding to all the tested values of N are provided. Once more, these simulations confirm the good performance of the channel estimation procedure and the robustness of the proposed DCT1e MCM scheme. Similar results (not shown here) have been obtained for the other channels considered in the previous section: indoor office channel A ($L = 32$, 6 non-null coefficients), indoor office channel B ($L = 71$, 6 non-null coefficients), pedestrian channel B ($L = 371$, 6 non-null coefficients), and vehicular channel A ($L = 252$, 6 non-null coefficients).

VII. CONCLUSIONS

In this work, we have introduced a novel DCT1e-based MCM transceiver which does not require the use of symmetric extension and any other transform (like the DFT) for the channel estimation and signal reconstruction stages. The general procedure for the estimation of an arbitrary channel's impulse response, without prior knowledge of its length, by means of the DCT1e has been described. In the transmitter, we have designed specific sparse training signals which are transformed in the receiver, using the so called MIRA procedure (a simple and efficient linear transformation), in order to estimate the channel. The theoretical conditions that guarantee perfect

TABLE V
ESTIMATED BER AS A FUNCTION OF THE SNR (DB) AND THE ORDER OF THE DCT1E USED (N) FOR ITU-R M.1225 PEDESTRIAN CHANNEL A. IN EACH COLUMN, THE FIRST RESULT CORRESPONDS TO ASSUMING A KNOWN CHANNEL AND THE SECOND ONE (IN PARENTHESES) TO THE ESTIMATED CHANNEL.

SNR (dB)	128	256	512	1024	2048
-10	0.4637 (0.5252)	0.4631 (0.5122)	0.4636 (0.5007)	0.4637 (0.4884)	0.4639 (0.4790)
-5	0.3881 (0.4639)	0.3813 (0.4343)	0.3828 (0.4185)	0.3790 (0.4014)	0.3848 (0.3985)
0	0.2854 (0.3570)	0.2861 (0.3310)	0.2810 (0.3082)	0.2766 (0.2931)	0.2851 (0.2955)
5	0.1909 (0.2453)	0.1922 (0.2247)	0.1887 (0.2083)	0.1835 (0.1956)	0.1857 (0.1910)
10	0.1133 (0.1469)	0.1139 (0.1342)	0.1123 (0.1250)	0.1166 (0.1230)	0.1105 (0.1135)
15	0.0652 (0.0843)	0.0620 (0.0732)	0.0687 (0.0755)	0.0634 (0.0670)	0.0679 (0.0704)
20	0.0366 (0.0487)	0.0369 (0.0428)	0.0404 (0.0437)	0.0341 (0.0361)	0.0401 (0.0411)
25	0.0221(0.0285)	0.0214 (0.0252)	0.0221 (0.0242)	0.0223 (0.0235)	0.0217 (0.0222)
30	0.0129 (0.0166)	0.0117 (0.0140)	0.0116 (0.0128)	0.0140 (0.0147)	0.0116 (0.0120)
35	0.0061 (0.0079)	0.0071 (0.0083)	0.0072 (0.0079)	0.0068 (0.0072)	0.0068 (0.0070)
40	0.0043 (0.0055)	0.0040 (0.0047)	0.0040 (0.0044)	0.0046 (0.0048)	0.0039 (0.0040)

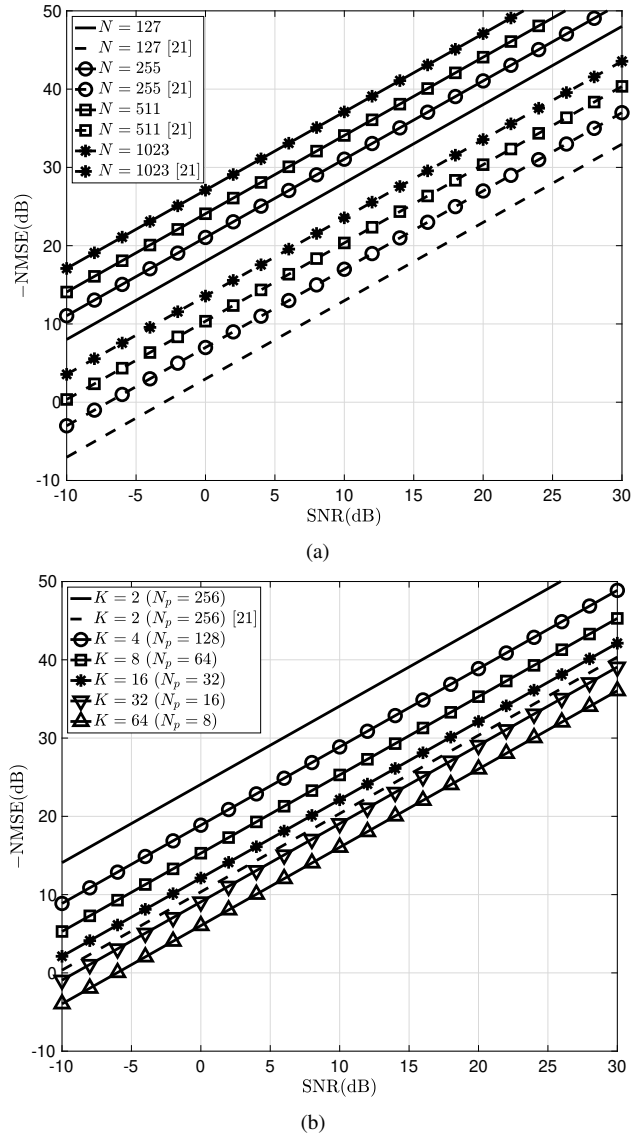

Fig. 8. Normalised mean squared error (NMSE(dB)) as a function of the signal power to noise ratio (SNR(dB)). (a) NMSE(dB) using $K = 2$ (i.e., $N_p = (N + 1)/K$) for different values of N using the proposed approach and the scheme proposed in [21]. (b) NMSE(dB) using $N = 511$ for different values of K using the proposed approach. Note that $-$NMSE(dB) is actually plotted in the figure, so higher values correspond to a better performance.

estimation of the channel's impulse response in the absence of noise have also been formulated. After the training stage, the signal reconstruction, i.e., the recovery of the transmitted zero–padded information symbols, is possible by applying again the MIRA procedure and performing channel equalization in the frequency domain. Numerical simulations show the excellent performance of the proposed approach, both in terms of channel estimation (measured by the reconstruction SNR) and signal reconstruction (measured by the BER). In future works we plan to carry out a detailed analysis of the performance of the proposed scheme in CFO, following the works of [3], [11] for the DCT2e and DCT4e, as well as the achievable data rate, following the works of [9], [33], [34], again for the DCT2e and DCT4e.

ACKNOWLEDGEMENTS

This work has been partially supported by the Spanish Ministry of Economy and Competitiveness through projects TEC2015-64835-C3-1-R and TEC2015-64835-C3-3-R, by Comunidad Autónoma de Madrid and by Universidad de Alcalá. M. E. Domínguez-Jiménez, D. Luengo and G. Sansigre-Vidal are members of UPM's TACA Research Group and would also like to thank Universidad Politécnica de Madrid (UPM) for its support. Finally, the authors would like to thank the Associate Editor and the anonymous Reviewers for their insightful recommendations, which have significantly contributed to the improvement of this paper.

REFERENCES

[1] J. A. C. Bingham, "Multicarrier modulation for data transmission: An idea whose time has come," *IEEE Communications Magazine*, vol. 28, no. 5, pp. 5–14, 1990.

[2] N. Al-Dhahir, H. Minn, and S. Satish, "Optimum DCT-based multicarrier transceivers for frequency-selective channels," *IEEE Transactions on Communications*, vol. 54, no. 5, pp. 911–921, 2006.

[3] P. Tan and N. C. Beaulieu, "A comparison of DCT-based OFDM and DFT-based OFDM in frequency offset and fading channels," *IEEE Transactions on Communications*, vol. 54, no. 11, pp. 2113–2125, 2006.

[4] F. Cruz-Roldán, M. E. Domínguez-Jiménez, G. Sansigre-Vidal, P. Amo-López, M. Blanco-Velasco, and Á. Bravo-Santos, "On the use of discrete cosine transforms for multicarrier communications," *IEEE Transactions on Signal Processing*, vol. 60, no. 11, pp. 6085–6090, 2012.

[5] B. Mathew, P. George, R. V. Nathan, S. Shukkor, and A. N. Lakshmi, "BER comparison of DCT and FFT based OFDM systems in AWGN and Rayleigh fading channels with different modulation schemes," in *2013 Annual International Conference on Emerging Research Areas and 2013 International Conference on Microelectronics, Communications and Renewable Energy*, 2013, pp. 1–4.

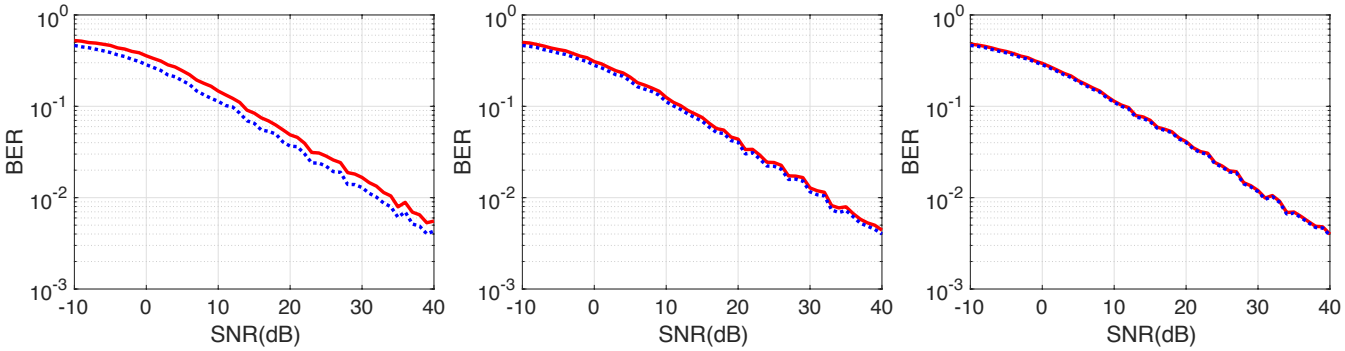

Fig. 9. Estimated BER for the pedestrian channel A of ITU-R M.1225 as a function of the SNR for several orders of the DCT1e. (a): $N = 128$. (b) $N = 512$. (c): $N = 2048$. In all cases, the blue dotted line shows the performance of the ideal system (which assumes a known channel) and the solid red line uses the estimated channel to construct the prefilter.

[6] F. Cruz-Roldán, M. E. Domínguez-Jiménez, G. Sansigre-Vidal, J. Piñeiro-Ave, and M. Blanco-Velasco, "Single-carrier and multicarrier transceivers based on discrete cosine transform type-IV," *IEEE Transactions on Wireless Communications*, vol. 12, no. 12, pp. 6454–6463, 2013.

[7] C. He, L. Zhang, J. Mao, A. Cao, P. Xiao, and M. A. Imran, "Performance analysis and optimization of DCT-based multicarrier system on frequency-selective fading channels," *IEEE Access*, vol. 6, pp. 13 075–13 089, 2018.

[8] C. He, A. Cao, L. Xiao, L. Zhang, P. Xiao, and K. Nikitopoulos, "Enhanced DCT-OFDM system with index modulation," *IEEE Transactions on Vehicular Technology*, vol. 68, no. 5, pp. 5134–5138, 2019.

[9] F. Cruz-Roldán, W. A. Martins, P. S. R. Diniz, and M. Moonen, "Achievable data rate of DCT-based multicarrier modulation systems," *IEEE Transactions on Wireless Communications*, vol. 18, no. 3, pp. 1739–1749, 2019.

[10] A. Cao, L. Xiao, P. Xiao, C. He, and R. Tafazolli, "A tight upper bound for enhanced DCT-OFDM with index modulation," *IEEE Transactions on Vehicular Technology*, vol. 69, no. 12, pp. 16 213–16 217, 2020.

[11] P. Amo-López, E. Domínguez-Jiménez, G. Sansigre, D. Sanz de la Fuente, and F. Cruz-Roldán, "Discrete cosine transform type-IV-based multicarrier modulators in frequency offset channels," in *2012 19th IEEE International Conference on Electronics, Circuits, and Systems (ICECS 2012)*, 2012, pp. 925–928.

[12] F. Cruz-Roldán, M. E. Domínguez-Jiménez, G. Sansigre-Vidal, D. Luengo, and M. Moonen, "DCT-based channel estimation for single-and multicarrier communications," *Signal Processing*, vol. 128, pp. 332–339, 2016.

[13] M. E. Domínguez-Jiménez, D. Luengo, and F. Cruz-Roldán, "Channel estimation using type-III even discrete cosine transform in multicarrier communications," in *IEEE Statistical Signal Processing Workshop (SSP)*, 2018, pp. 498–502.

[14] Y. Liu, Z. Tan, H. Hu, L. J. Cimini, and G. Y. Li, "Channel estimation for OFDM," *IEEE Communications Surveys & Tutorials*, vol. 16, no. 4, pp. 1891–1908, 2014.

[15] M. K. Ozdemir and H. Arslan, "Channel estimation for wireless OFDM systems," *IEEE Communications Surveys & Tutorials*, vol. 9, no. 2, pp. 18–48, 2007.

[16] Y.-H. Yeh and Sau-GeeChen, "Efficient channel estimation based on discrete cosine transform," in *IEEE International Conference on Acoustics, Speech, and Signal Processing (ICASSP)*, vol. 4, 2003, pp. 676–679.

[17] M. Diallo, R. Rabineau, and L. Cariou, "Robust DCT based channel estimation for MIMO-OFDM systems," *IEEE Wireless Communications and Networking Conference (WCNC)*, pp. 1–5, 2009.

[18] A. Nycil and E. G. Anoop, "A new DCT based channel estimation algorithm for OFDM systems," *International Journal of Computer Applications*, vol. 58, pp. 26–30, 2012.

[19] X. Xiong, B. Jiang, X. Gao, and X. You, "DCT-based channel estimator for OFDM systems: threshold setting and leakage estimation," in *IEEE International Conference on Wireless Communications and Signal Processing*, 2013, pp. 1–5.

[20] M. E. Domínguez-Jiménez, D. Luengo, and G. Sansigre-Vidal, "Estimation of symmetric channels for discrete cosine transform type-I multicarrier systems: A compressed sensing approach," *The Scientific World Journal*, vol. 2015, 2015.

[21] M. E. Domínguez-Jiménez, D. Luengo, G. Sansigre-Vidal, and F. Cruz-Roldán, "A novel channel estimation scheme for multicarrier communications with the type-I even discrete cosine transform," in *25th European Signal Processing Conference (EUSIPCO)*, 2017, pp. 2239–2243.

[22] M. E. Domínguez-Jiménez, G. Sansigre-Vidal, and D. Luengo, "Signal reconstruction in multicarrier comunications by means of the discrete cosine transform type-III even," in *41st International Conference on Telecommunications and Signal Processing (TSP)*, 2018, pp. 1–4.

[23] M. E. Domínguez-Jiménez, D. Luengo, and G. Sansigre-Vidal, "Channel estimation based on the discrete cosine transform type-III even," in *26th European Signal Processing Conference (EUSIPCO)*, 2018, pp. 1297–1301.

[24] M. E. Domínguez-Jiménez, G. Sansigre-Vidal, D. Osés, and D. Luengo, "On the feasibility of SISO/MIMO-PLC based on the discrete cosine transform type-III even," in *42nd International Conference on Telecommunications and Signal Processing (TSP)*, 2019, pp. 566–570.

[25] F. Cruz-Roldán, F. A. Pinto-Benel, M. E. Domínguez-Jiménez, and G. Sansigre-Vidal, "Single-carrier frequency division multiple access with discrete cosine transform type-I," in *IEEE 13th International New Circuits and Systems Conference (NEWCAS)*, 2015, pp. 1–4.

[26] S. A. Martucci, "Symmetric convolution and the discrete sine and cosine transforms," *IEEE Transactions on Signal Processing*, vol. 42, no. 5, pp. 1038–1051, 1994.

[27] V. Sánchez, P. García, A. M. Peinado, J. C. Segura, and A. J. Rubio, "Diagonalizing properties of the discrete cosine transforms," *IEEE Transactions on Signal Processing*, vol. 43, no. 11, pp. 2631–2641, 1995.

[28] S. G. Johnson and M. Frigo, "A modified split-radix FFT with fewer arithmetic operations," *IEEE Transactions on Signal Processing*, vol. 55, no. 1, pp. 111–119, 2007.

[29] S. M. Perera and J. Liu, "Complexity reduction, self/completely recursive, radix-2 DCT I/IV algorithms," *Journal of Computational and Applied Mathematics*, vol. 379, pp. 1–16, 2020.

[30] F. Cruz-Roldán, J. Piñeiro-Ave, J. Rojo-Álvarez, and M.Blanco-Velasco, "Simple algorithms for estimating the symbol timing offset in DCT-based multicarrier systems," *Wireless Communications and Mobile Computing*, vol. 2018, 2018, Article ID 3649513, 8 pages.

[31] M. E. Domínguez-Jiménez, "Full spark of even discrete cosine transforms," *Signal Processing*, vol. 176, p. 107632, Nov. 2020. [Online]. Available: https://doi.org/10.1016/j.sigpro.2020.107632

[32] "Guidelines for evaluation of radio transmission technologies for IMT-2000," *ITU-R Rec. M*, vol. 1225, 1997.

[33] W. A. Martins, F. Cruz-Roldán, M. Moonen, and P. S. Ramirez Diniz, "Intersymbol and intercarrier interference in OFDM transmissions through highly dispersive channels," in *2019 27th European Signal Processing Conference (EUSIPCO)*, 2019, pp. 1–5.

[34] F. Cruz-Roldán, W. A. Martins, F. García G., M. Moonen, and P. S. R. Diniz, "Intersymbol and intercarrier interference in OFDM systems: Unified formulation and analysis," *arxiv:2012.04527v1*, 2020.